Route LINKER

5105-135
Solar Thermal Power Systems Project
Parabolic Dish Systems Development

DOE/JPL-1060-73
Distribution Category UC-62

# The Kinematic Stirling Engine as an Energy Conversion Subsystem for Paraboloidal Dish Solar Thermal Power Plants

J.M. Bowyer

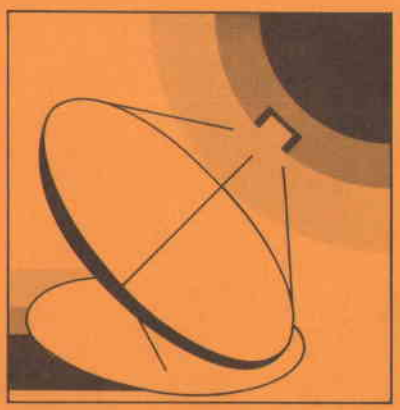

April 15, 1984

Prepared for
U.S. Department of Energy
Through an Agreement with
National Aeronautics and Space Administration
by
Jet Propulsion Laboratory
California Institute of Technology
Pasadena, California

JPL Publication 84-30

5105-135
Solar Thermal Power Systems Project
Parabolic Dish Systems Development

DOE/JPL-1060-73
Distribution Category UC-62

# The Kinematic Stirling Engine as an Energy Conversion Subsystem for Paraboloidal Dish Solar Thermal Power Plants

J.M. Bowyer

April 15, 1984

Prepared for
U.S. Department of Energy
Through an Agreement with
National Aeronautics and Space Administration
by
Jet Propulsion Laboratory
California Institute of Technology
Pasadena, California

JPL Publication 84-30

Prepared by the Jet Propulsion Laboratory, California Institute of Technology, for the U.S. Department of Energy through an agreement with the National Aeronautics and Space Administration.

The JPL Solar Thermal Power Systems Project is sponsored by the U.S. Department of Energy and is part of the Solar Thermal Program to develop low-cost solar thermal and electric power plants.

## ABSTRACT

The potential of a suitably designed and economically manufactured Stirling engine as the energy conversion subsystem of a paraboloidal dish-Stirling solar thermal power module has been estimated.

Results obtained by elementary cycle analyses have been shown to match quite well the performance characteristics of an advanced kinematic Stirling engine, the United Stirling P-40, as established by current prototypes of the engine and by a more sophisticated analytic model of its advanced derivative.

In addition to performance, brief consideration has been given to other Stirling engine criteria such as durability, reliability, and serviceability. Production costs have not been considered here.

## FOREWORD

A few years ago, an investigation was undertaken as part of a comparative study of promising advanced power conversion subsystems suitable for use in paraboloidal dish solar thermal power systems. The results of this investigation are reported herein. These results have been recently reviewed and are considered currently applicable. Ultimately, the Stirling engine and other selected types of engines will be compared on the basis of performance, durability, reliability, serviceability, and cost criteria. The potential rewards and risks associated with future technological and economic developments that affect these criteria must also be reassessed in each case.

## ACKNOWLEDGMENT

The work described herein was conducted by the Jet Propulsion Laboratory, California Institute of Technology, for the U.S. Department of Energy through an agreement with the National Aeronautics and Space Administration (NASA Task RE-152, Amendment 327; DOE/ALO/NASA Interagency Agreement No. DE-AM04-80AL13137).

CONTENTS



Figures

# SECTION I

# INTRODUCTION

A few years ago, an intensive effort was made to determine the potential of a suitably designed and economically manufactured Stirling-cycle engine as the energy conversion subsystem of a point-focusing, cavity-receiver solar thermal power module. Currently, the module of greatest interest comprises a paraboloidal collector that is pointed continuously at the sun and carries a cavity receiver and power conversion unit at its focus; however, the applicability of the Stirling-cycle engine is not limited to this particular configuration.

As with the Carnot cycle, the ideal Stirling cycle is reversible and, thus, has the highest thermal efficiency attainable when operated between prescribed temperatures of source and sink. Yet, as is also true for the Carnot cycle, no practical engine has yet been devised that operates on the ideal Stirling cycle.

Some practical engines operate on one or the other of a variety of cycles that approximate the ideal Stirling cycle. Unfortunately, each of these practical engines incorporates apparently unavoidable design features that limit the compression ratio of the engine and introduce thermodynamic irreversibilities and mechanical losses; as a result, the thermal efficiency of these practical engines is universally less -- frequently much less -- than that of a reversible engine operating between the same temperatures of source and sink.

An equally troublesome set of limitations that has persistently retarded the development of a practical Stirling-cycle engine consists of (1) the sliding seals required for pistons and the sliding or rolling seals required for piston rods, (2) the oil contamination that fouls regenerators in particular and the entire working space of the engine in general when piston and/or piston rod seals leak, (3) the high cost of fabricating regenerators and heaters that are highly effective at the moderately high cyclic speeds required to obtain a high specific power-to-volume or power-to-weight ratio, (4) the high mean working pressure required for a compact engine, (5) the kinds and quantities of metals and/or ceramics required to allow operation at source temperatures high enough to provide an engine power density and efficiency competitive with internal combustion engines, and (6) the relatively large cooling system required to reject the heat from this closed-cycle engine as compared with open-cycle engines.

Certain attractive features of a practical engine operating on a cycle that approximates the Stirling cycle have served to stimulate a sustained interest in this concept in the face of all the problems noted above. Some of these features are (1) potentially high thermal efficiency, (2) quietness and smoothness of operation, and (3) an ability to utilize a variety of fuels with relatively less resultant atmospheric pollution than that generated by a comparable internal combustion engine.

The following sections of this report discuss (1) the Stirling and quasi-Stirling cycles and simulation of these cycles, (2) the limitations that currently circumscribe the practicality of so-called Stirling engines and the probability that these limitations may be relaxed or removed, and (3) an attempt to assess the potential of the practical quasi-Stirling engine as the power conversion subsystem for a point-focusing cavity-receiver, solar thermal power module.

## A. OBJECTIVES

In view of the remarks presented in preceding paragraphs, the following objectives were defined for this investigation:

(1) Determination of the principal parameters affecting Stirling engine performance and assessment of the sensitivity of performance to variations in these parameters.

(2) Estimation of the potential of the kinematic Stirling engine in terms of the following criteria: performance, durability, reliability, and serviceability. Mass production costs have been addressed in a separate study (Ref. 1). (Thermodynamic cycle analysis, examination of the above-named criteria as they apply to recent and currently existing Stirling engines, and projection of these criteria for future engines that incorporate promising new theoretical and technological innovations have each contributed to the results presented here.)

(3) Suggestion of a development plan that offers the probability of considerable improvement in kinematic Stirling engines as measured by the stated criteria.

## B. BACKGROUND

Earlier studies (Refs. 2, 3, and 4) noted the potentially high performance capability of Stirling engines; however, these studies also noted the relatively undeveloped state of this type of engine as compared, for example, with those of the Rankine- and Brayton-cycle engines. Of the two general types of Stirling engine, kinematic and free piston, the free piston type was assumed to have the higher ultimate potential, but to be less well developed than the kinematic type. Thus, the kinematic type Stirling engine was chosen as the more viable power conversion unit for initial paraboloidal dish-Stirling solar thermal power plants (Ref. 5).

Two existing kinematic Stirling engines, viz., the United Stirling P-40 and the Phillips I-98, were adapted to serve as the power conversion subsystems in first-generation paraboloidal dish-Stirling solar thermal power module designs. Even these engines could not be considered to be fully developed at the time this study was done; thus, they served in the study reported here only as the base from which the criteria for future engines have been projected.

## SECTION II

## THE STIRLING CYCLE -- DISCUSSION AND ANALYSIS

### A. DESCRIPTIONS AND DEFINITIONS

Two rather different general configurations for Stirling-cycle engines have been developed. The kinematic configuration, like the usual Otto- or Diesel-cycle engine, converts the linearly oscillatory motion of the power piston to steady rotational motion of a shaft. In the free-piston configuration, the oscillatory linear motion of the power piston can be directly imposed on a coaxial extension of the piston rod that, in turn, drives some linearly oscillating load, e.g., the armature of a linear electric alternator.

The kinematic configuration is represented by two major versions, viz., the dual-piston version and the piston-displacer version. In turn, two variants of the piston-displacer version exist. Figure 2-1, taken from Reference 6, defines these three kinematic configurations.

Figure 2-2 presents the pressure-volume diagrams for the simple regenerative Stirling cycle and for the regenerative Stirling cycle with regenerator dead volume. Point 4' of the latter cycle has been made coincident with point 4 of the former in order to provide a definite basis for comparison in the following discussion.

Figure 2-3 presents the sequence of processes constituting the cycle for a dual-piston, double-acting (Rinia-type) Stirling engine. Such an engine usually comprises four cylinders connected in a ring arrangement.

Figure 2-4 presents the sequence of processes constituting the cycle for a Beta-type piston-displacer Stirling engine.

Elementary thermodynamic analysis of the ideal Stirling cycle is relatively simple; however, because the ideal cycle only crudely represents the thermodynamic cycle on which any practical Stirling engine operates, the results of the elementary analysis are of little practical significance. In order to provide an introduction to the development of a second, more elaborate model and to provide a reference with which that second model can be compared, the indicated efficiency and work performance parameter of the simple regenerative Stirling cycle is presented here.

The ideal Stirling cycle consists of a series of four discrete processes (cf. Figure 2-2): an isothermal compression from thermodynamic state ($p_1$, $V_1$, $T_1$) to thermodynamic state ($p_2$, $V_2$, $T_2 = T_1$), a constant-volume heat addition from thermodynamic state ($p_2$, $V_2$, $T_2$) to thermodynamic state ($p_3$, $V_3 = V_2$, $T_3$), an isothermal expansion from thermodynamic state ($p_3$, $V_3$, $T_3$) to thermodynamic state ($p_4$, $V_4$, $T_4 = T_3$), and a constant volume heat rejection from thermodynamic state ($p_4$, $V_4$, $T_4$) back to the original thermodynamic state ($p_1$, $V_1 = V_4$, $T_1$).

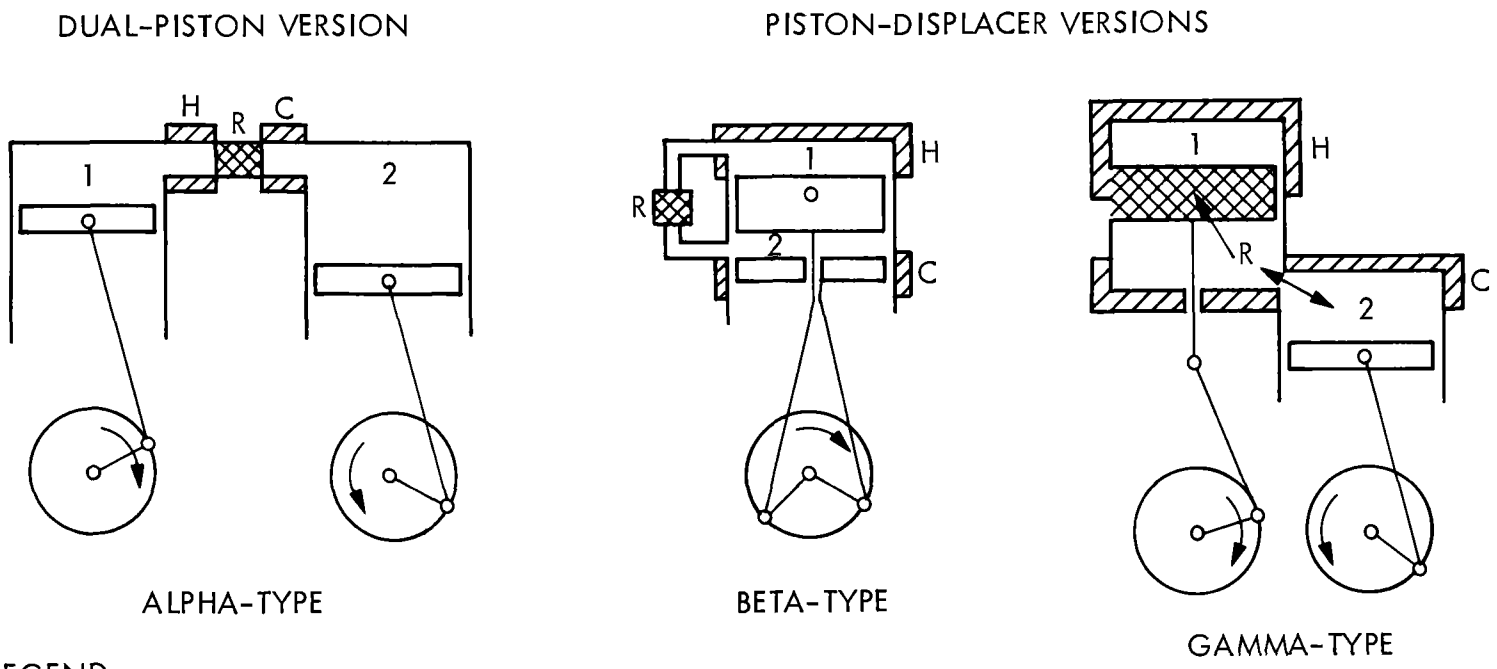


Figure 2-1. Stirling Engine Kinematic Configurations

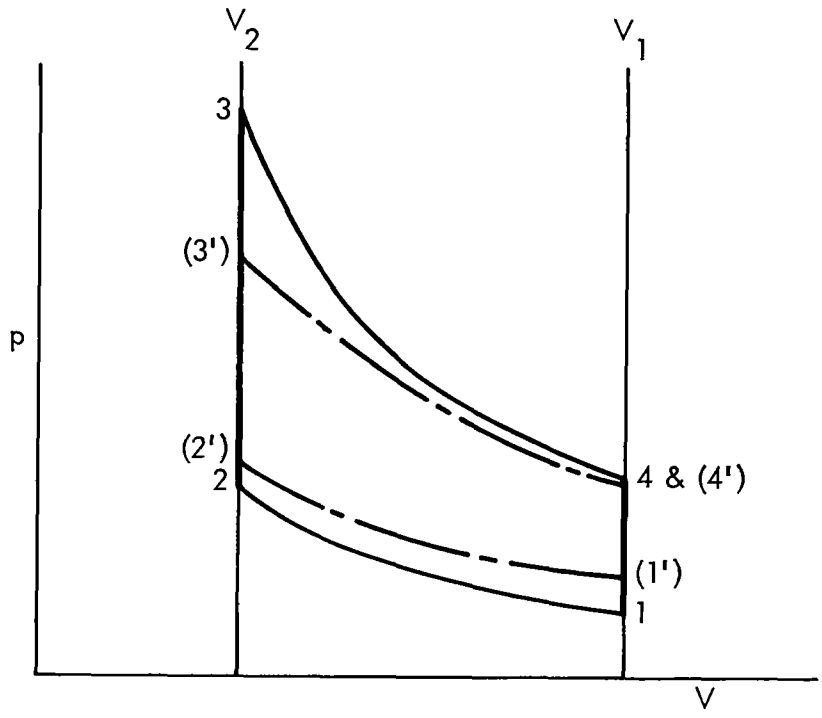


Figure 2-2. Simple, Perfectly Regenerative Stirling Cycle: 1-2-3-4-1; Perfectly or Imperfectly Regenerative Stirling Cycle with Regenerator Dead Volume: 1'-2'-3'-4'-1' (Note: $V_4' = V_4$ and $p_4' = p_4$.)

When regeneration is perfect, the thermodynamic efficiency of the ideal Stirling cycle is equal to that of the Carnot cycle when both cycles are operated between the same temperatures of source and sink. This efficiency is expressed by the familiar formula,

$$\eta_{s\ (ideal)} = \eta_{Carnot} = 1 - \frac{T_C}{T_H} . \qquad (1)$$

This is shown in the discussion of the simple regenerative Stirling cycle that appears in the following section of this report.

The ideal Stirling cycle analysis presumes the ability to satisfy several thermodynamic conditions that are not physically realistic. Among these are the following:

(1) During the expansion or compression process, all of the thermodynamic medium is assumed to be at temperature $T_H$ or $T_C$, respectively. Thus, the ideal cycle fails to allow for those

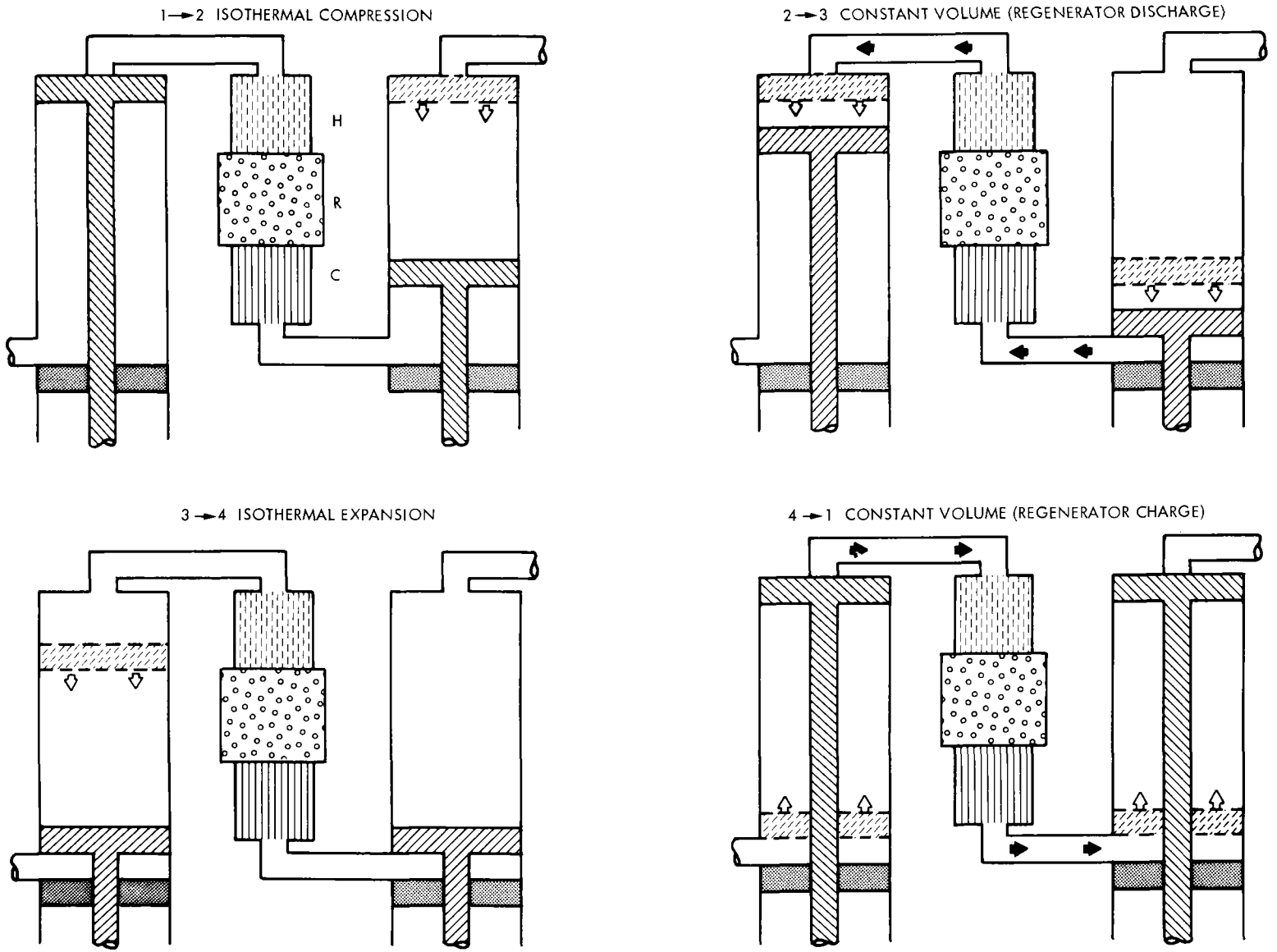


Figure 2-3. Dual-Piston Stirling Cycle Comprising Four Distinct Processes

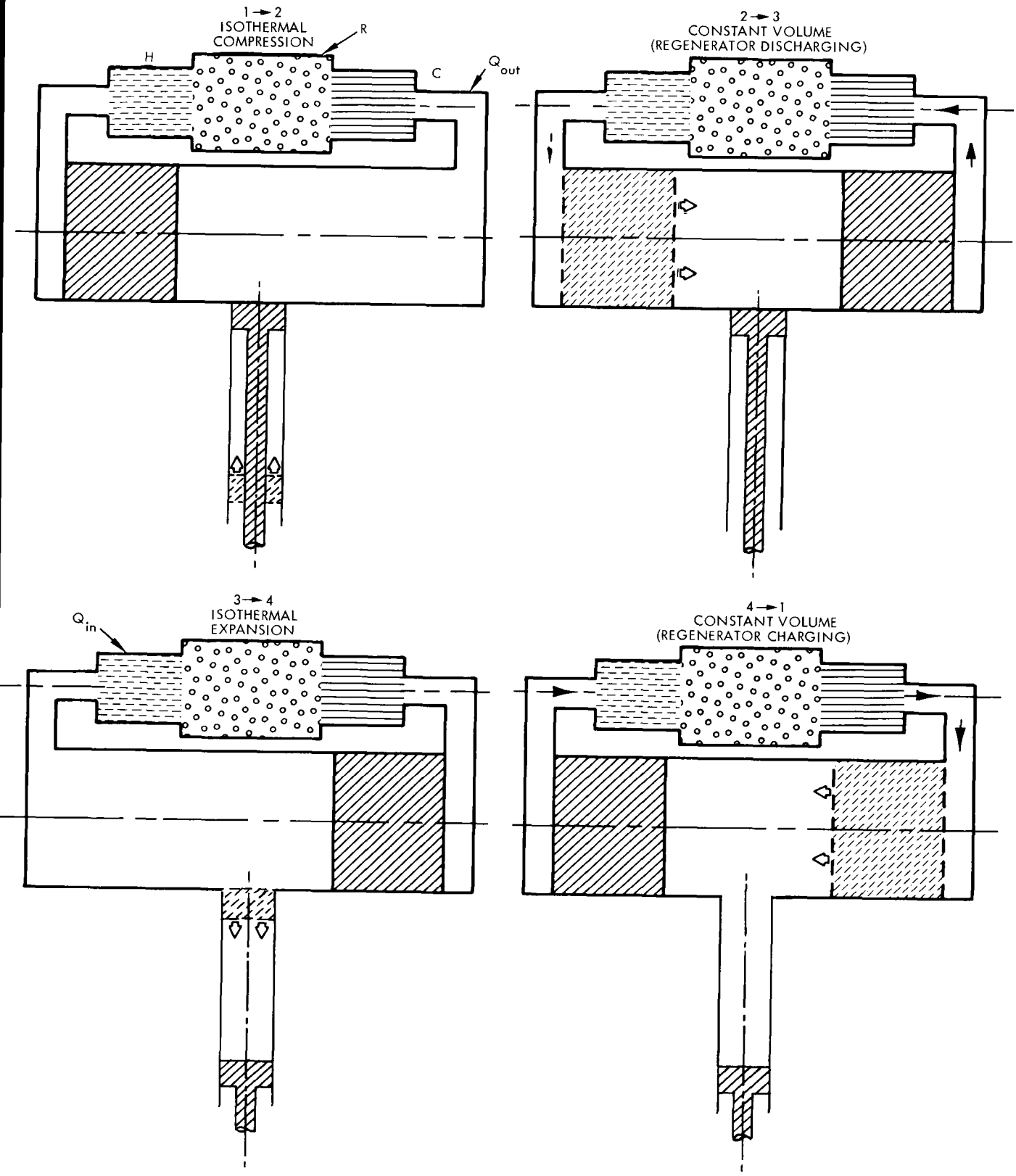


Figure 2-4. Piston-Displacer Stirling Cycle Comprising Four Distinct Processes

volumes of the dead space within the cooler at temperature $T_C$ during the expansion process, within the heater at temperature $T_H$ during the compression process, or within the regenerator at varying temperatures intermediate to $T_H$ and $T_C$ during either process.

Furthermore, unless elaborate efforts are made to maintain a more or less uniform, constant temperature of the medium that is undergoing expansion or compression within the hot and cold spaces, the gas in these spaces will be subject to processes that are more nearly adiabatic than isothermal.

(2) During the constant-volume heat addition and removal processes of the cycle, all of the thermodynamic medium is assumed to be at one common temperature at any instant, even though some of the working fluid must again reside in the cooler at temperature $T_C$, in the heater at temperature $T_H$, and in the regenerator at various intermediate temperatures.

(3) No actual materials are perfect insulators or, at ordinary temperatures, perfect conductors. Because any of the usual thermodynamic media must be contained at elevated temperatures and pressures during at least part of any practical thermodynamic cycle, boundaries of finite strength and corresponding thickness are required. Heat leaks and heat transfers across finite temperature differences occur at these boundaries; these processes are thermodynamically irreversible and therefore result in reduced cycle efficiency.

(4) All flow processes within the working space are assumed to occur without loss, i.e., the thermal conductivity of the fluid is assumed to be infinite, yet the closely related viscosity of the medium is assumed to be zero. Unless the thermodynamic processes of the cycle all proceed at infinitesimal rates, the ideal cycle cannot be realized when any real thermodynamic medium is used.

## B. ANALYSIS

### 1. Evaluation of the Simple Regenerative Stirling Cycle

a. Zero Dead Volume; Perfect or Imperfect Regeneration. The work accomplished by a reversible, isothermal process is given by the formula,

$$W = mRT \ln \frac{V_f}{V_i} . \qquad (2)$$

Applied to the expansion and compression processes of the Stirling cycle,

$$W_E = mRT_H \ln \frac{V_4}{V_3} = mRT_H \ln \frac{V_1}{V_2} \tag{3}$$

and

$$W_C = mRT_C \ln \frac{V_2}{V_1} = - mRT_C \ln \frac{V_1}{V_2} , \tag{4}$$

respectively. The net work per cycle is, thus,

$$W_{net} = W_E + W_C = mRT_H \left(1 - \frac{T_C}{T_H}\right) \ln \frac{V_1}{V_2} . \tag{5}$$

The thermal energy furnished to the engine per cycle consists of the thermal equivalent of the work of expansion plus the constant-volume heat addition required to compensate for imperfect regeneration:

$$Q_{in} = mC_v(T_H - T_R) + W_E. \tag{6}$$

Defining regenerator effectiveness as

$$E = \frac{T_R - T_C}{T_H - T_C} ,$$

$$1 - \frac{T_R}{T_H} = (1 - E)\left(1 - \frac{T_C}{T_H}\right). \tag{7}$$

After algebraic manipulation, $Q_{in}$ can now be expressed as:

$$Q_{in} = mRT_H \left[\frac{1 - E}{k - 1}\left(1 - \frac{T_C}{T_H}\right) + \ln \frac{V_1}{V_2}\right] . \tag{8}$$

Cycle efficiency can now be determined:

$$\eta = \frac{W_{net}}{Q_{in}}$$

or

$$\eta = \left(1 - \frac{T_C}{T_H}\right) \frac{\ln \frac{V_1}{V_2}}{\left[\frac{1 - E}{k - 1}\left(1 - \frac{T_C}{T_H}\right) + \ln \frac{V_1}{V_2}\right]} . \tag{9}$$

Obviously, when regeneration is perfect, E = 1 and

$$\eta = \left(1 - \frac{T_C}{T_H}\right) = \eta_{Carnot} . \tag{10}$$

Defining the cycle work performance parameter as

$$P_w = \frac{W_{net}}{p_1(V_1 - V_2)} \tag{11}$$

and substituting appropriately,

$$P_w = \frac{\left(1 - \frac{T_C}{T_H}\right) \ln \frac{V_1}{V_2}}{\frac{T_C}{T_H}\left(1 - \frac{V_2}{V_1}\right)} . \tag{12}$$

Note that here the minimum cycle pressure, $p_1$, has been employed in the definition of $P_w$.

b. Finite Dead Volume; Perfect or Imperfect Regeneration. In a practical Stirling-cycle engine, that part of the volume occupied by the working medium but not swept by pistons is termed the "dead space." Dead space comprises the piston clearance volumes, the heater, regenerator, and cooler net internal volumes, and the volume of the connecting ducts. A thermodynamic analysis that is slightly more elaborate than the most elementary retains the concept of a series of distinct thermodynamic processes but allows consideration of the dead space as well as of regenerator effectiveness. This second method of analysis provides a considerably more accurate model for the performance of a practical Stirling engine. The trends of indicated engine efficiency and indicated work performance parameter as functions of regenerator effectiveness and/or dead volume are correctly indicated. Still, the analysis employs lumped parameters and distinct thermodynamic processes, so, at best, the resulting model must be calibrated to the corresponding practical Stirling engine before useful quantitative results can be obtained.

This second model has been the primary analytic tool of this study. The much greater complexity of the next significantly higher level of analysis, i.e., the second-order methods, prevented its application to the problem at hand at this time; nevertheless, the glaring weaknesses of the model employed here must be admitted, and the results obtained from it must be circumspectly evaluated.

2. Regenerative Stirling Cycle with Regenerator Dead Space

First, consider the discharge of the regenerator. Assume that the regenerator discharge process results in the advance from one end of the regenerator to the other of a discontinuous drop in temperature from the cycle source temperature to the cycle sink temperature as shown in Figure 2-5. Further assume that a constant average pressure exists in the regenerator during this process (this as an approximation).

Under these approximations, the time-averaged mass of gas contained in the regenerator void volume resulting from this discharge process will be

$$m_R = \frac{\bar{p}}{R} \int_0^{V_R} \frac{dv}{T} , \tag{13}$$

where T, the instantaneous average temperature of the gas in the regenerator void volume, is given by

$$T = T_C + \left(1 - \frac{v}{V_R}\right)(T_H - T_C) . \tag{14}$$

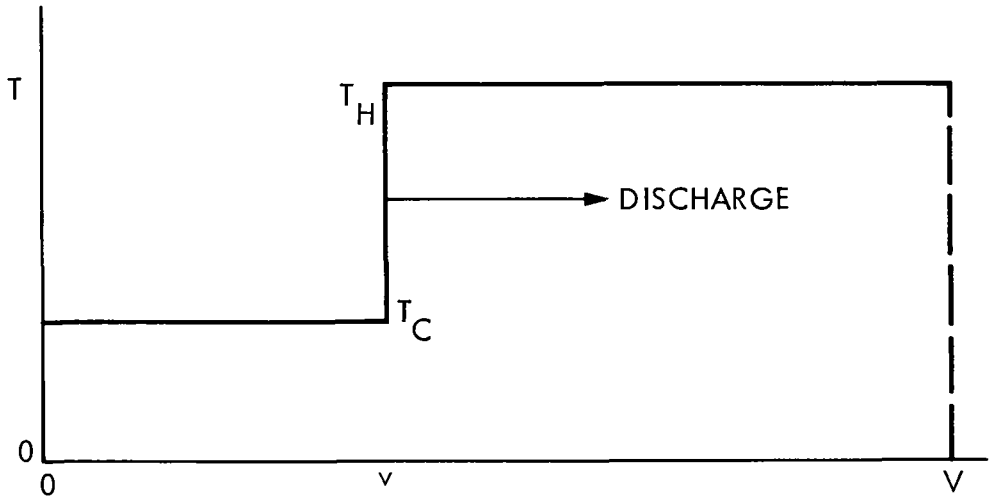


Figure 2-5. Ideal Regenerator Discharge

Substituting for T and integrating over $V_R$,

$$m_R = \frac{\bar{p}\ V_R}{R(T_H - T_C)} \ln \frac{T_H}{T_C} . \tag{15}$$

Defining a time-averaged regenerator temperature, $T_R$,

$$m_R = \frac{\bar{p}\ V_R}{R\ T_R} , \tag{16}$$

whence,

$$T_R = \frac{T_H - T_C}{\ln \frac{T_H}{T_C}} . \tag{17}$$

The charging of a regenerator can be considered in an exactly corresponding way and results in the same expression for $T_R$.

Several subtle but appreciable approximations are hidden in this derivation of a representative time-averaged regenerator temperature; some of these are

(1) It is assumed that the regenerator discharging or charging process is complete. This cannot be precisely true.

(2) Use of this average regenerator temperature implies that the regenerator is always either charging or discharging. This is untrue because, at certain phases of the cycle, the thermal energy in the regenerator remains virtually constant at either the extreme high level (fully charged) or the extreme low level (completely discharged).

(3) The thermal capacity of either the heating or cooling gas and the heat transfer coefficient between either heating or cooling gas and the regenerator matrix are all finite.

(4) The step increase or decrease in temperature in the regenerator is dispersed by axial conduction in the regenerator matrix.

(5) Part of the thermal energy stored in the regenerator as a result of the charging process is lost by thermal leakage.

(6) A constant average pressure during the charging or discharging was assumed in obtaining the log-mean temperature difference for $T_R$; however, in the following development, $T_R$ will be employed in a formula for instantaneous pressure during the same charging or discharging process. The effect of this approximation is unclear.

A second, more conventional approach to determining the time-averaged mass and mean temperature of the gas in the regenerator utilizes the analysis of H. Hausen (Ref. 7). A translation of the most pertinent parts of this reference is appended. Hausen showed that the mean spatial distribution of the temperature in the matrix is linear and constant under the following assumptions:

(1) Equal thermal capacities and half-cycle times for the heating and cooling gases.

(2) Negligible end effects (end effects are small in the usual regenerator).

(3) Large thermal capacity of the matrix relative to those of the gases.

(4) Negligible axial conduction in the matrix.

(5) Constant heat transfer coefficient between the gases and the matrix.

Under these conditions, Hausen also showed the temporal mean temperature difference between the heating gas and the matrix to be (1) equal to that between the matrix and the cooling gas and (2) constant.

If the further assumption is made that the heat transfer coefficient between either gas and the matrix is very large, the temperature difference between gas and matrix will be relatively small. The temporally constant distribution of the gas mean temperature can then be written as

$$T = T_C + \frac{v}{V_R} (T_H - T_C). \tag{18}$$

Assuming a constant average pressure in the regenerator, as was done in the first case, it can again be shown that

$$m_R = \frac{\bar{p}\, V_R}{R\, T_R},$$

where

$$T_R = \frac{T_H - T_C}{\ln \frac{T_H}{T_C}}.$$

This same result has been presented previously by Martini (Ref. 6) and Berchowitz (Ref. 8). Comparison of these two analyses based on radically different assumptions shows the results for $T_R$ to be identical and strongly reinforces the author's belief that $T_R$ is probably relatively insensitive to the choice of regenerator model.

In spite of the inaccuracies imposed by using a constant log-mean temperature difference to represent a time-dependent average regenerator temperature, the indicated efficiency and work performance parameter of the resulting model have been shown a posteriori to be reasonably accurate when the limited parameters of the model are determined by calibration of the model relative to experimental results and other more elaborate models.

During the isothermal expansion process in this more complicated model, the working gas inventory is represented by

$$m' = \frac{p'}{R}\left(\frac{V_H}{T_H} + \frac{V_R}{T_R}\right). \tag{19}$$

(Note that no allowance has been made in this model for any void volume at the sink temperature, even though practical Stirling engines require some clearance volume at the cold end of the working space and, at least in contemporary engines, some volume in the cooler.)

Solving for p',

$$p' = \frac{m'R}{\frac{V_H}{T_H} + \frac{V_R}{T_R}}. \tag{20}$$

Determining the work of expansion

$$W'_E = \int_{V_2}^{V_1} \frac{m'Rdv}{\frac{V}{T_H} + \frac{V_R}{T_R}}$$

$$= m'RT_H \ln\left(\frac{\frac{V_1}{T_H} + \frac{V_R}{T_R}}{\frac{V_2}{T_H} + \frac{V_R}{T_R}}\right)$$

$$= m'RT_H \ln\left(\frac{\frac{T_R}{T_H} + \frac{V_R}{V_1}}{\frac{T_R}{T_H}\frac{V_2}{V_1} + \frac{V_R}{V_1}}\right). \tag{21}$$

Determining the work of compression in a similar way,

$$W'_C = \int_{V_1}^{V_2} \frac{m'Rdv}{\frac{V}{T_C} + \frac{V_R}{T_R}}$$

$$= m'RT_C \ln \left( \frac{\frac{V_2}{T_C} + \frac{V_R}{T_R}}{\frac{V_1}{T_C} + \frac{V_R}{T_R}} \right)$$

$$= m'RT_C \ln \left( \frac{\frac{T_R}{T_H}\frac{V_2}{V_1} + \frac{T_C}{T_H}\frac{V_R}{V_1}}{\frac{T_R}{T_H} + \frac{T_C}{T_H}\frac{V_R}{V_1}} \right) . \qquad (22)$$

Determining the thermal energy added per cycle,

$$Q'_{in} = m'C_v (T_H - T_R) + W_E$$

$$= m'RT_H \left\{ \ln \left( \frac{\frac{T_R}{T_H} + \frac{V_R}{V_1}}{\frac{T_R}{T_H}\frac{V_2}{V_1} + \frac{V_R}{V_1}} \right) + \frac{1-E}{k-1} \left( 1 - \frac{T_C}{T_H} \right) \right\} . \qquad (23)$$

The indicated efficiency of this model can now be determined:

$$\eta' = \frac{\left(1 - \frac{T_C}{T_H}\right) \cdot \frac{\ln\left(\frac{\frac{T_R}{T_H} + \frac{T_C}{T_H}\frac{V_R}{V_1}}{\frac{T_R}{T_H}\frac{V_2}{V_1} + \frac{T_C}{T_H}\frac{V_R}{V_1}}\right)}{\ln\left(\frac{\frac{T_R}{T_H} + \frac{V_R}{V_1}}{\frac{T_R}{T_H}\frac{V_2}{V_1} + \frac{V_R}{V_1}}\right)}}{1 + \frac{\frac{(1 - E)}{(k - 1)}\left(1 - \frac{T_C}{T_H}\right)}{\ln\left(\frac{\frac{T_R}{T_H} + \frac{V_R}{V_1}}{\frac{T_R}{T_H}\frac{V_2}{V_1} + \frac{V_R}{V_1}}\right)}} \quad . \tag{24}$$

From the above equation, it can be seen that if

$$E = 1 \text{ and } \frac{V_R}{V_1} = 0 \ ,$$

then

$$\eta' = 1 - \frac{T_C}{T_H} = \eta_{Carnot} \ .$$

Also it can be seen that when

$$\frac{T_C}{T_H} = 1 \ ,$$

then

$$\eta' = \eta_{Carnot} = 0 \ .$$

The latter case is, of course, trivial.

In all other practical cases, even when E = 1, if

$$\frac{V_2}{V_1} < 1 \ ,$$

$$\frac{T_C}{T_H} < 1 \ ,$$

and

$$\frac{V_R}{V_1} > 0 \ ,$$

then

$$\eta' < \eta_{Carnot} .$$

The work performance parameter for the regenerative Stirling cycle with regenerator dead space is defined as

$$P'_w = \frac{W'_{net}}{p'_1 (V_1 - V_2)} \ . \qquad (25)$$

Thus, the form is exactly the same as that employed in the case of the simple regenerative Stirling cycle.

As in Reference 6, the pressure, $p_4'$, at the end of the isothermal expansion stroke in the regenerative Stirling cycle with regenerator dead space has been made equal to the pressure, $p_4$, of the same point in the simple regenerative Stirling cycle. The rationale for this choice is that $p_4$ and $p_4'$ closely approximate the temporal mean pressure of the corresponding model, and, for a specified $T_H$, creep strength based on temporal mean pressure is the criterion that determines the wall thicknesses of the cylinder head, heater tubes, and other hot-end pressure-retaining components.

It is possible to show by a rather tedious analysis that, given $p_4' = p_4$,

$$\frac{m'}{m} = 1 + \frac{V_R/V_1}{T_R/T_H} \quad , \tag{26}$$

$$\frac{p_1'}{p_1} = \frac{\frac{T_R}{T_H} + \frac{V_R}{V_1}}{\frac{T_R}{T_H} + \frac{T_C}{T_H}\frac{V_R}{V_1}} \quad , \tag{27}$$

$$\frac{p_2'}{p_2} = \frac{V_2}{V_1} \cdot \frac{\frac{T_R}{T_H} + \frac{V_R}{V_1}}{\frac{T_R}{T_H}\frac{V_2}{V_1} + \frac{T_C}{T_H}\frac{V_R}{V_1}} \quad , \tag{28}$$

and

$$\frac{p_3'}{p_3} = \frac{V_2}{V_1} \cdot \frac{\frac{T_R}{T_H} + \frac{V_R}{V_1}}{\frac{T_R}{T_H}\frac{V_2}{V_1} + \frac{V_R}{V_1}} \quad . \tag{29}$$

Whether regeneration is perfect or imperfect, the ratio of the net works performed, henceforth denoted simply by W'/W, is given by

$$\frac{W'}{W} = \left(1 + \frac{\frac{V_R}{V_1}}{\frac{T_R}{T_H}}\right) \cdot \frac{\ln\left(\frac{\frac{T_R}{T_H} + \frac{V_R}{V_1}}{\frac{T_R}{T_H}\frac{V_2}{V_1} + \frac{V_R}{V_1}}\right) - \frac{T_C}{T_H}\ln\left(\frac{\frac{T_R}{T_H} + \frac{T_C}{T_H}\frac{V_R}{V_1}}{\frac{T_R}{T_H}\frac{V_2}{V_1} + \frac{T_C}{T_H}\frac{V_R}{V_1}}\right)}{\left(1 - \frac{T_C}{T_H}\right)\ln\frac{V_1}{V_2}} \quad . \tag{30}$$

Now, resuming the discussion of $P_w'$, comparison shows that

$$\frac{P_w'}{P_w} = \frac{W'/W}{p_1'/p_1} \quad , \tag{31}$$

and, substituting for W'/W and $p_1'/p_1$ leads to the relation

$$\frac{P_w'}{P_w} = \left(1 + \frac{\frac{T_C}{T_H}\frac{V_R}{V_1}}{\frac{T_R}{T_H}}\right) \cdot \frac{\ln\left(\frac{\frac{T_R}{T_H} + \frac{V_R}{V_1}}{\frac{T_R}{T_H}\frac{V_2}{V_1} + \frac{V_R}{V_1}}\right) - \frac{T_C}{T_H}\ln\left(\frac{\frac{T_R}{T_H} + \frac{T_C}{T_H}\frac{V_R}{V_1}}{\frac{T_R}{T_H}\frac{V_2}{V_1} + \frac{T_C}{T_H}\frac{V_R}{V_1}}\right)}{\left(1 - \frac{T_C}{T_H}\right)\ln\frac{V_1}{V_2}} \quad . \tag{32}$$

The maximum working volume of the regenerative Stirling engine with regenerator dead space is $V_{max} = V_1 + V_R$, while the minimum working volume of the engine is $V_{min} = V_2 + V_R$. It follows from these two equations that

$$\frac{V_R}{V_{max}} = \frac{\frac{V_R}{V_1}}{1 + \frac{V_R}{V_1}} \quad \text{or} \quad \frac{V_R}{V_1} = \frac{\frac{V_R}{V_{max}}}{1 - \frac{V_R}{V_{max}}} \tag{33}$$

and

$$\frac{V_{max}}{V_{min}} = \frac{1 + \frac{V_R}{V_1}}{\frac{V_2}{V_1} + \frac{V_R}{V_1}} \quad \text{or} \quad \frac{V_2}{V_1} = \frac{1 - \frac{V_R}{V_{min}}}{\frac{V_{max}}{V_{min}} - \frac{V_R}{V_{min}}} \quad . \tag{34}$$

Of course, still other volume ratios could be defined; however, the important point to note here is that definition of the simple regenerative Stirling cycle requires the specification of k, $T_C/T_H$, $V_2/V_1$, $V_R/V_1$, and E. In the case of the simple cycle, $V_2/V_1 = V_{min}/V_{max}$; in the case of the more complicated cycle, the two volume ratios $V_2/V_1$ and $V_R/V_1$ can be replaced by $V_{max}/V_{min}$ and $V_R/V_{min}$ if desired.

The effect of regenerator dead space on cycle performance is perhaps best illustrated by a specific example. If it is assumed that k = 1.4, $T_C/T_H = 1/3$, $V_2/V_1 = 1/2$, and E = 1, the results presented in Figure 2-6 are obtained.

In the preparation of this graph, the assumption of equal average working space pressure at the end of the expansion strokes of the engines without and with regenerator dead space was made. Note that the work ratio, W'/W, and the efficiency ratio, $\eta'/\eta_{Carnot}$, decrease nearly linearly with increasing ratio of regenerator volume to maximum working space volume.

The effects of variations in k, $T_C/T_H$, $V_{max}/V_{min}$, $V_R/V_{min}$, and E on the regenerative Stirling cycle with regenerator dead space have been explored parametrically. Results of this parametric evaluation of the model are presented in Figures 2-7 through 2-11. In Figure 2-11, $\eta_M$ represents the mechanical efficiency of the engine.

Because of the heat transfer and thermal energy storage requirements of the heater, regenerator, and cooler components coupled with the requirement for reasonably low pressure losses in these same components, there exists a practical maximum limit to volume compression ratio, $V_{max}/V_{min}$. Walker (Ref. 9) has estimated this limit to be $V_{max}/V_{min} \approx 2.5$. The corresponding maximum for the ratio of regenerator dead volume to minimum volume is 1.0; however, this can occur only if regenerator dead volume and minimum volume are equal! This is not a practical possibility because of (1) the necessity for displacing the minimum volume of working gas through the regenerator in order to discharge the regenerator and, thus, to heat the gas at constant volume during this phase of the thermodynamic cycle and (2) the required finite volumes of the heater and the cooler. After considering these practical requirements, it was concluded that a practical maximum value for the ratio of regenerator dead space to minimum volume in a conventional Stirling engine is approximately one-half.

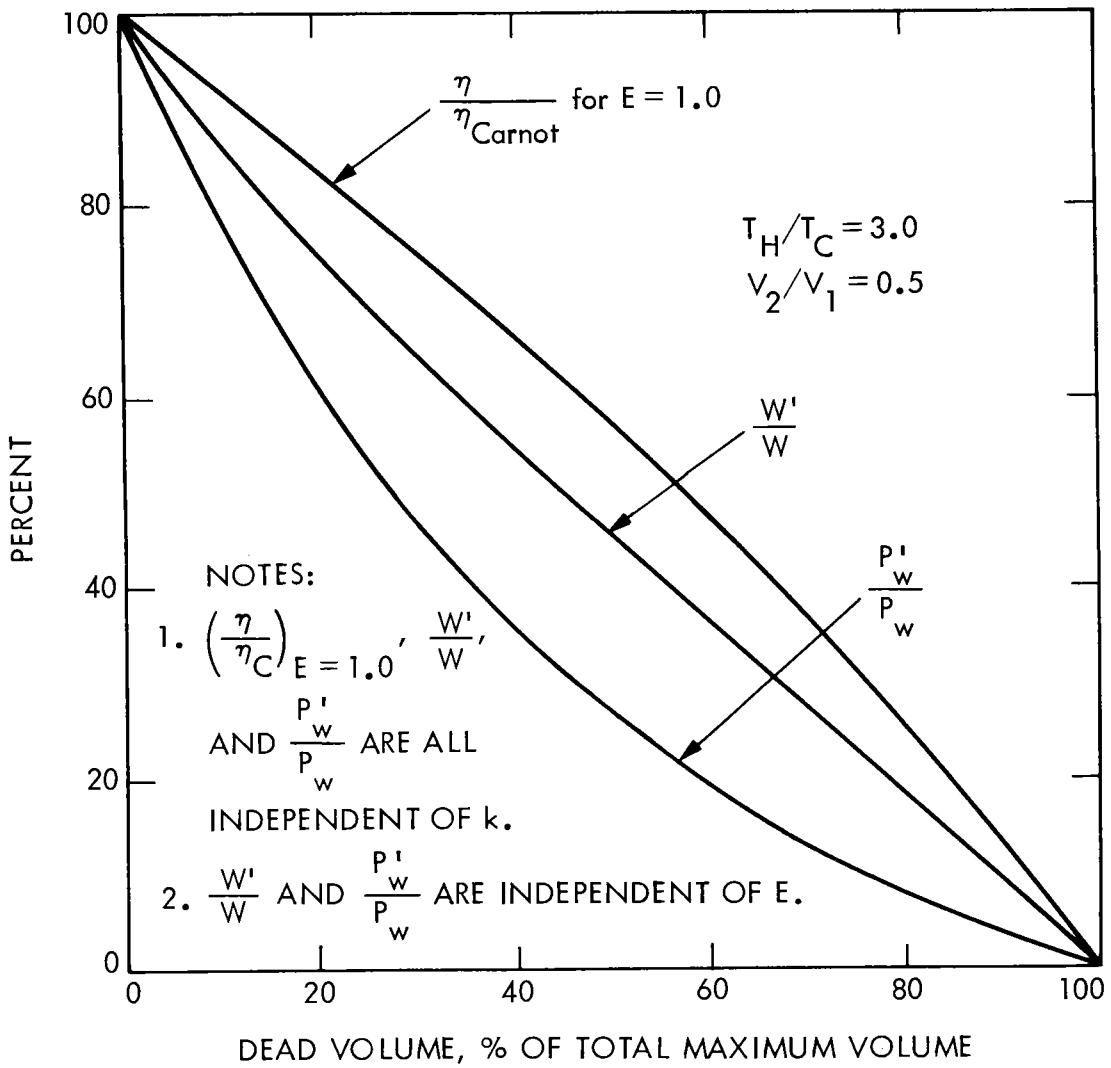


Figure 2-6. Effect of Dead Volume on Discrete-Process Stirling Cycle Performance

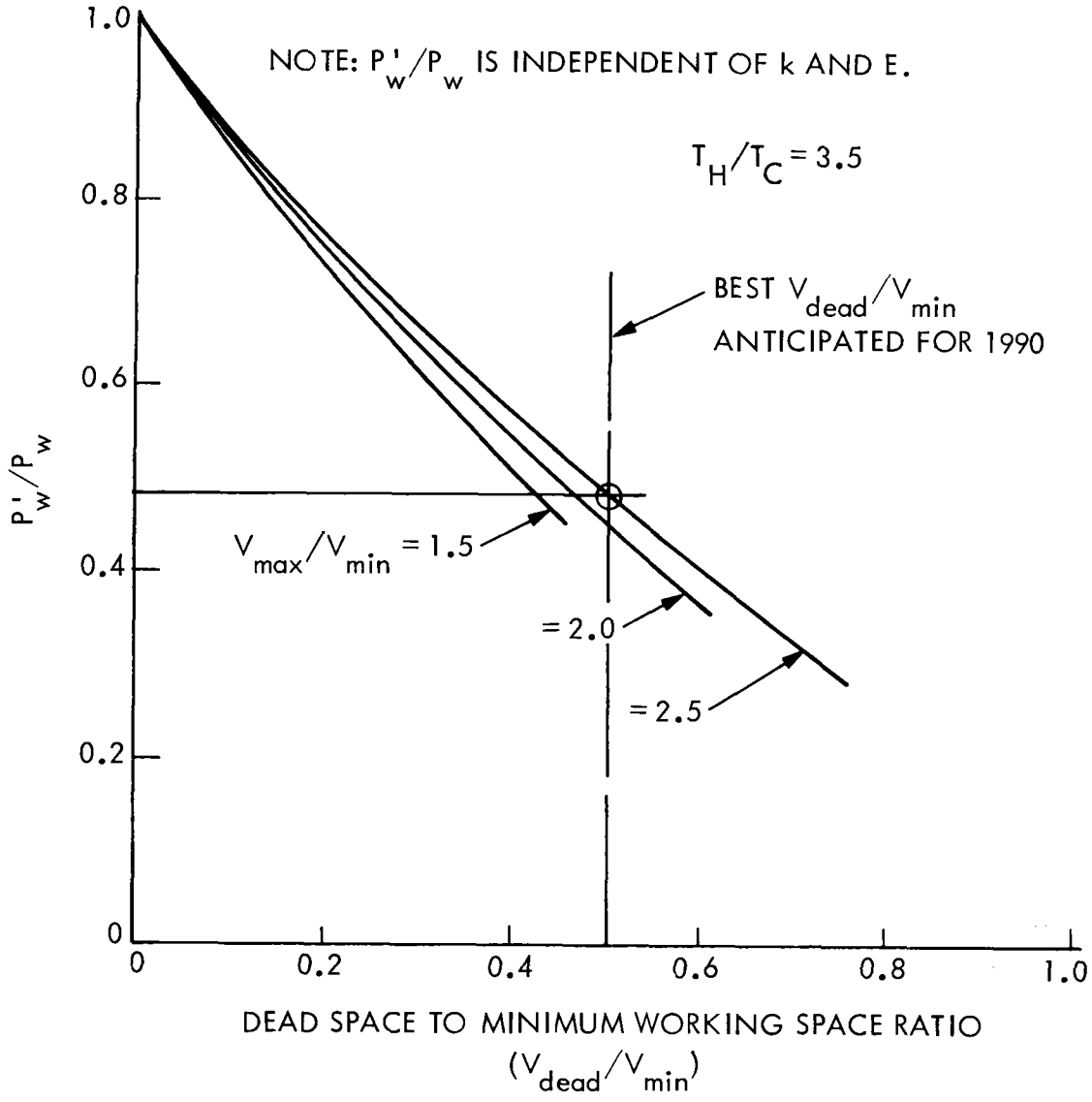


Figure 2-7. Normalized Work Performance Parameter as a Function of Dead Space to Minimum Working Space Ratio for a Discrete-Process Stirling Cycle

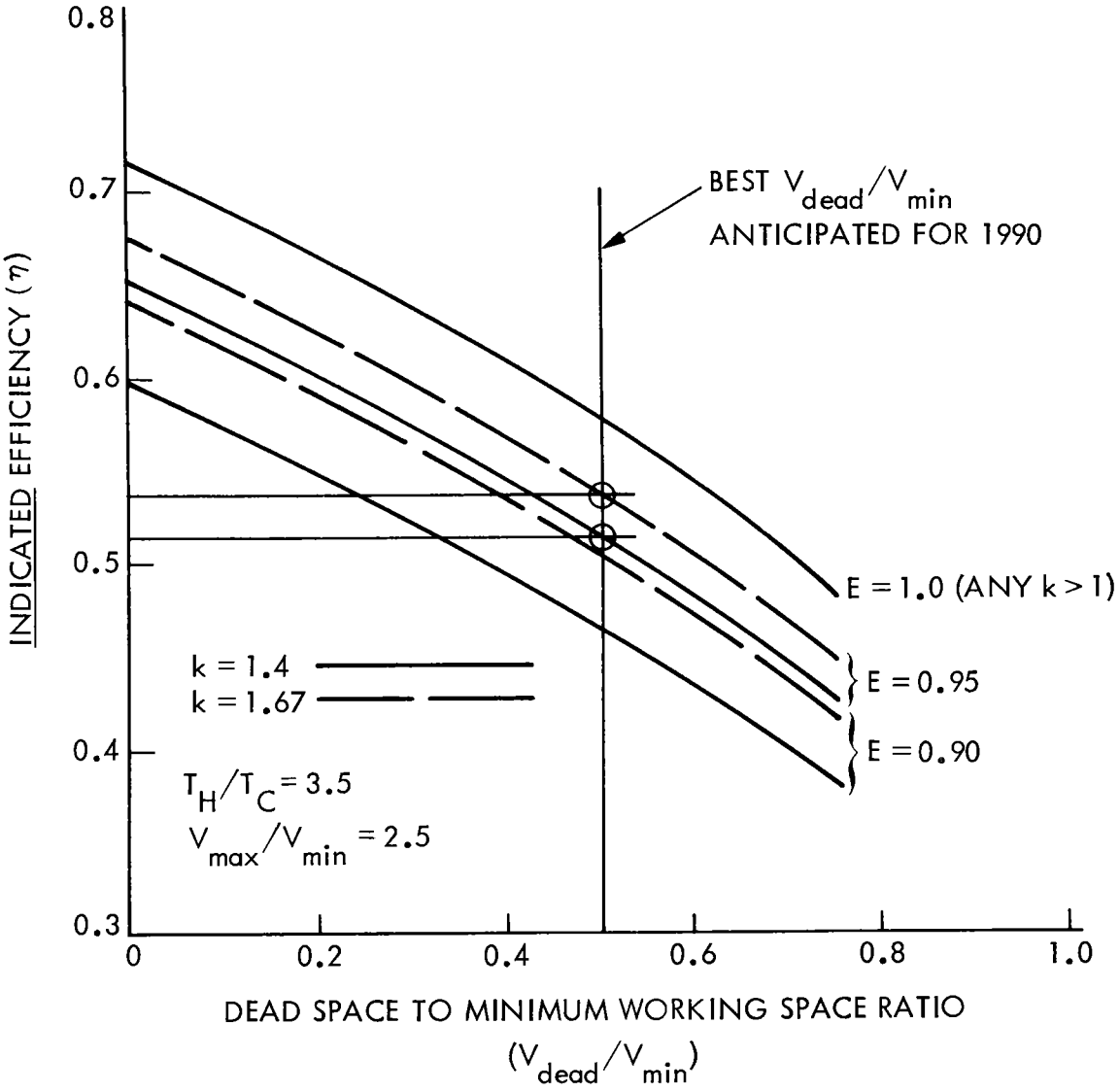


Figure 2-8. Indicated Efficiency as a Function of Dead Space to Minimum Working Space Ratio for a Discrete-Process Stirling Cycle

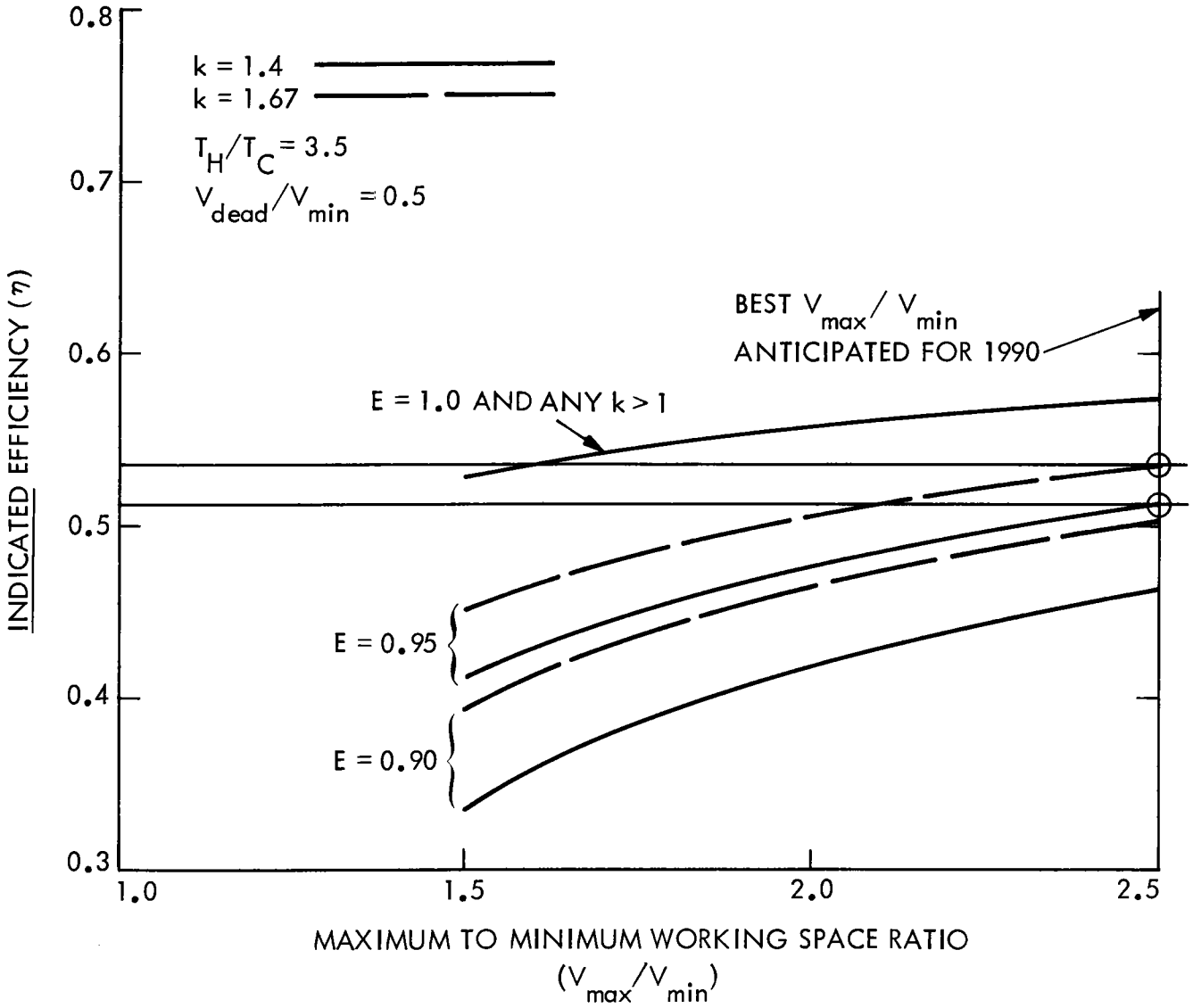


Figure 2-9. Indicated Efficiency as a Function of Maximum to Minimum Working Space Ratio for a Discrete-Process Stirling Cycle

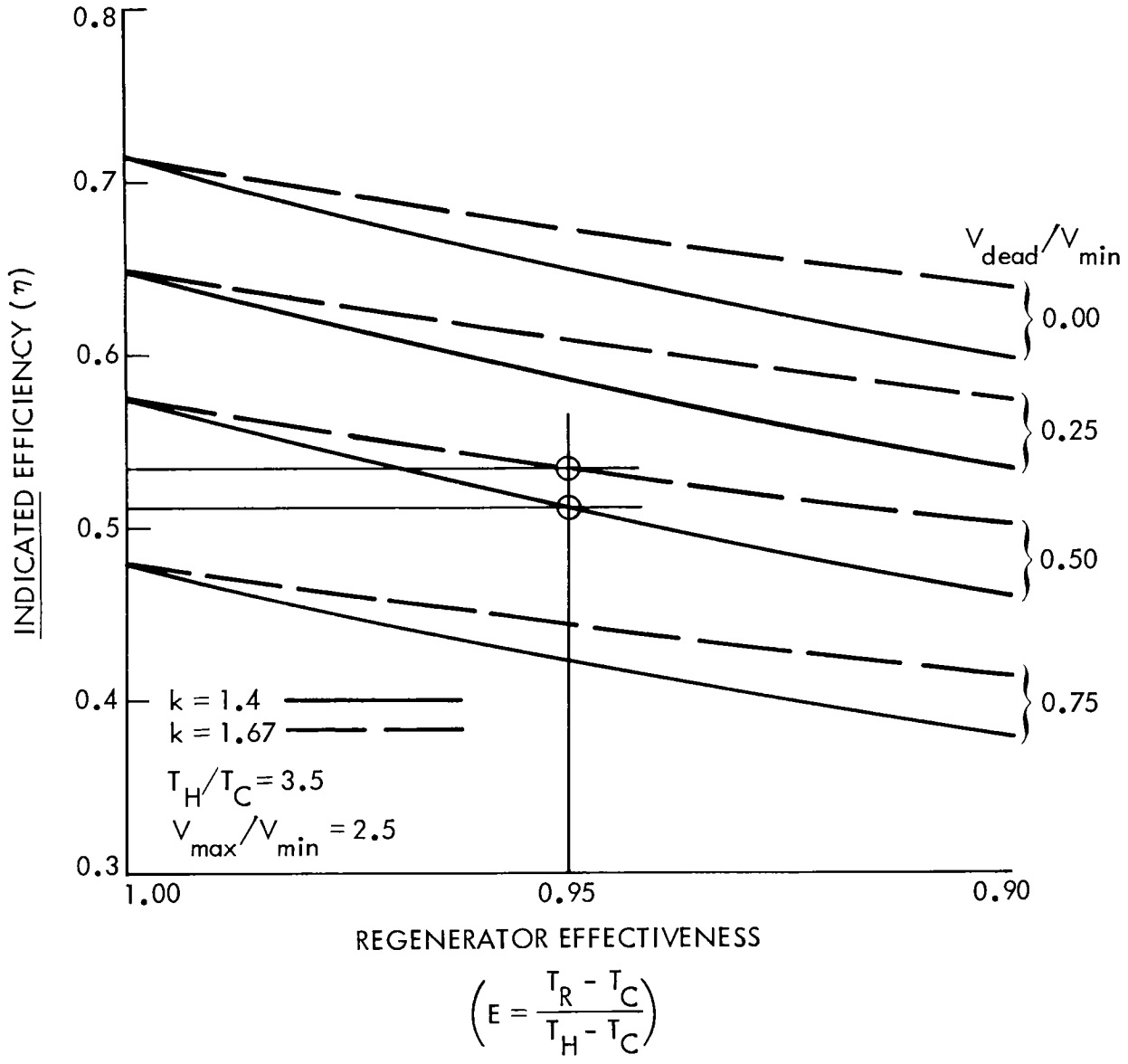


Figure 2-10. Effect of Regenerator Effectiveness on Stirling Cycle Efficiency for a Discrete-Process Stirling Cycle

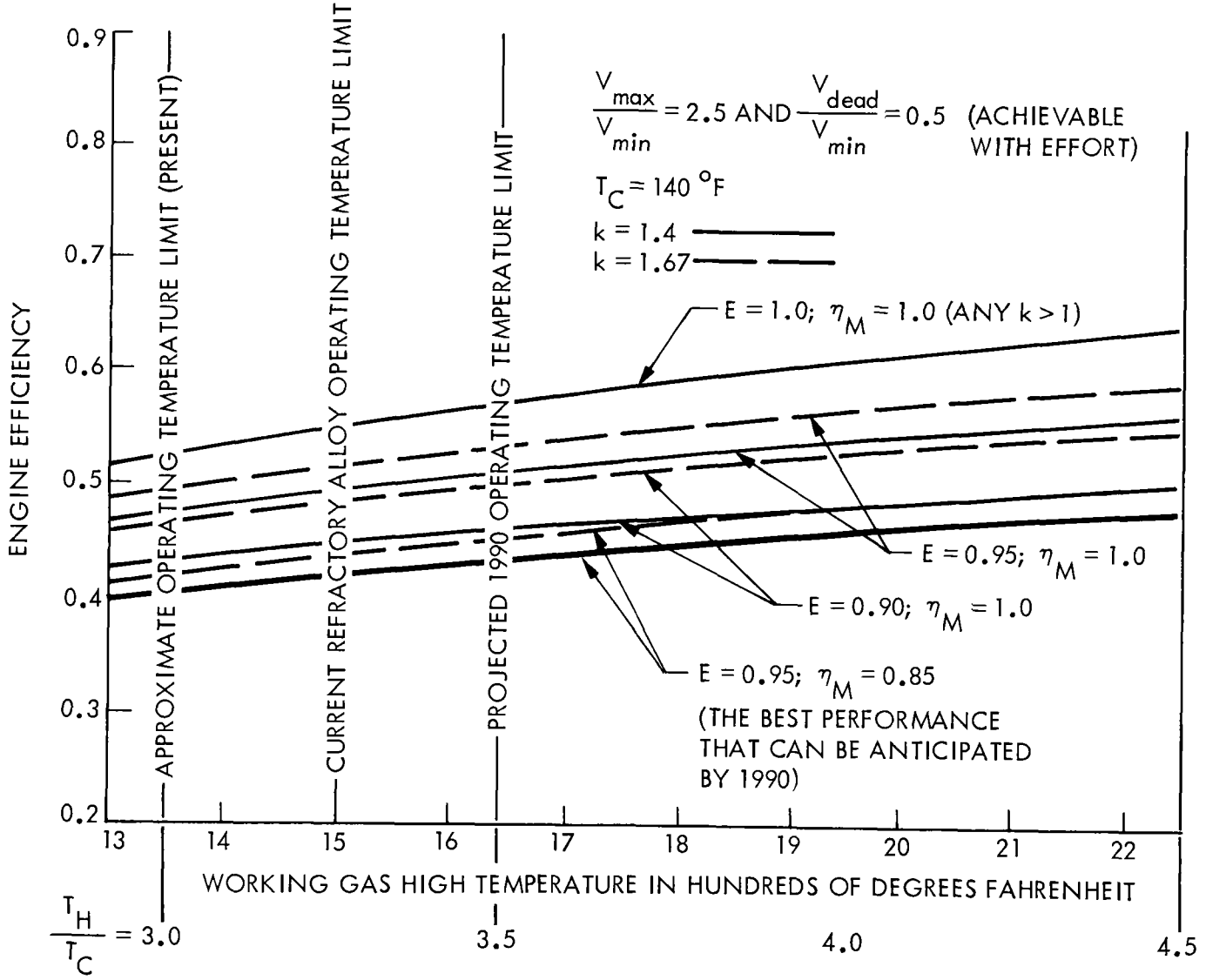


Figure 2-11. Stirling Engine Efficiency as a Function of Working Gas High Temperature for a Discrete-Process Stirling Cycle

## C. EVALUATION OF RESULTS OBTAINED FROM THE MODEL

The pronounced effect of dead volume to minimum volume ratio, $V_{dead}/V_{min}$, on work performance is indicated in Figure 2-7. At $V_{dead}/V_{min} = 0.5$, an almost one percent degradation in normalized work performance parameter, $P_w'/P_w$, results from each one percent increase in $V_{dead}/V_{min}$. This degradation is more pronounced at smaller values of $V_{dead}/V_{min}$ and smaller values of the maximum to minimum volume ratio, $V_{max}/V_{min}$, although, over the ranges of these parameters shown in the figures, the effect due to $V_{max}/V_{min}$ is obviously less than the effect due to $V_{dead}/V_{min}$.

As shown in Figure 2-8, the sensitivity of indicated efficiency, $\eta$, to $V_{dead}/V_{min}$ is only about two-thirds as large as the sensitivity of $P_w'/P_w$ to $V_{dead}/V_{min}$ in the vicinity of the representative engine points; however, the marked increase in this sensitivity at increasing values of $V_{dead}/V_{min}$ should be noted.

The effect of maximum to minimum working space ratio, $V_{max}/V_{min}$, on $\eta$ is presented in Figure 2-9; the sensitivity of $\eta$ to $V_{max}/V_{min}$ is not large in the vicinity of the engine points used in the example, but this sensitivity is greater at smaller values of $V_{max}/V_{min}$.

Because of the scales selected for the ordinate and abscissa of Figure 2-10, the sensitivity of $\eta$ to regenerator effectiveness, E, may not appear impressive; however, in the vicinity of the sample engine points, a degradation of more than one percent in $\eta$ results from a one percent decrease in E when the working medium is a diatomic gas and a two-thirds percent decrease in $\eta$ with a one percent decrease in E when the medium is a monatomic gas.

From Figures 2-8, 2-9, 2-10, and 2-11, the observant reader may have noted that the indicated engine efficiency obtained by using a monatomic medium is apparently better than that obtained by using a diatomic medium when regeneration is less than perfect, i.e., $E<1$. Actual Stirling engines almost universally employ either helium (monatomic) or hydrogen (diatomic) as the working medium, and, in the same engine, hydrogen often results in a slightly higher efficiency than does helium. Both hydrogen and helium are employed because of their low molecular weights and associated excellent heat transfer and low flow loss characteristics; in these respects, hydrogen is superior to helium. However, the analytic model employed herein does not account for heat transfer and flow loss effects, and, thus, helium (being monatomic) exhibits its thermodynamic advantage over hydrogen when regenerator effectiveness is less than one. There appears to be a consensus that, when all factors are considered, either of these two gases in a suitably optimized variant of the same engine would result in about the same efficiency as the other.

Engine efficiency (indicated or brake, as noted on particular curves) is presented as a function of working gas high temperature in Figure 2-11. Regenerator effectiveness, E, and the ratio of specific heats of the working medium, k, also appear as parameters in this figure. Note that this figure pertains to one sample engine ($V_{max}/V_{min} = 2.5$ and $V_{dead}/V_{min} = 0.5$)

that is rejecting heat to a thermodynamic sink at 140°F. The principal characteristics of the Stirling engine that are indicated by Figure 2-11 are the following:

(1) High regenerator efficiency becomes increasingly important as the working gas high temperature is increased.

(2) When regenerator effectiveness is imperfect, the thermodynamic advantage of helium over hydrogen that is indicated by the model employed here becomes increasingly important as the working gas high temperature is increased.

(3) The magnitude of the kinematic Stirling engine brake efficiency predicted for a regenerator effectiveness of 0.95 at 1500°F working gas high temperature is in close agreement with the performance predicted for the improved United Stirling P-40 and P-75 engines, viz., $\eta \approx 40\%$. Furthermore, insofar as can be determined at present, the trend of this efficiency with increasing working gas high temperature approximates the predicted performance of advanced technology derivatives of these same engines.

## D. HIGHER-ORDER METHODS OF STIRLING-CYCLE ANALYSIS

In order to consider the more realistic quasi-Stirling cycle corresponding to the sinusoidal motions of the pistons and the resulting overlapping thermodynamic processes, so-called first-order and second-order methods of analysis have been developed, cf. Ref. 6. These methods may be either numerical or analytic; however, numerical analysis allows the more general consideration of regenerator storage characteristics. As customarily applied, only the work performed per cycle and the work performance parameter are calculated on a strictly analytic basis. The indicated cycle efficiency is estimated by applying what is termed an experience factor to the Carnot efficiency corresponding to the given temperatures of source and sink, and the cycle brake efficiency is estimated by applying a second experience factor, the mechanical efficiency, to the indicated cycle efficiency. The two experience factors vary with the type of Stirling engine, its method of construction, the operating temperatures, etc.; thus, these factors are heavily dependent on experience and must be determined from existing data.

While this method has been applied in the course of the current study, no results are presented here because of the tenuously empirical nature of the method.

Also in this study, an initial attempt was made to employ the very sophisticated third-order numerical program published by Tew, et al., (Ref. 10) for analysis of the Stirling engine; however, this attempt was terminated for the following reasons:

(1) As written, the program was applicable only to piston-displacer-type engines.

(2) Numerical values for many of the engine design parameters were inserted directly into the program rather than through input lists, and the values inserted were uniquely representative of the GM GPU-3-2.

(3) As a result of two keypunch errors at JPL that could not be detected by the computer diagnostic program, correct operation of the Stirling program was obtained only after tedious and time-consuming examination and too late to be utilized in this study.

Of the models described above, only the model of Tew, et al., and other similar sophisticated numerical models can emulate Stirling engine performance and efficiency without a heavy dependence upon empirically established correction factors.

## E. FURTHER REMARKS

No practical thermodynamic engine has ever demonstrated an efficiency equal to that of its corresponding idealized cycle; in fact, the practical utility of thermodynamic engines has, in the past, depended as much on the ability of the actual engine to approach the corresponding ideal as on the efficiency of that ideal cycle to approach the corresponding Carnot efficiency. The present techno-economic domination of practical Rankine-, Otto-, Diesel-, and Brayton-cycle engines, to the almost total exclusion of practical Ericsson-, Stirling-, or Carnot-cycle engines, is obvious. Yet the ideal thermodynamic efficiency of each of the three engine types that have thus far dominated industry is less than that of the Ericsson, Stirling, and Carnot engines.

While the thermodynamic efficiency of any heat engine is of great interest, the work performed per cycle, per unit time, per unit volume, and per unit mass is of at least equal interest. The ideal efficiency of the Carnot cycle is the highest attainable at given temperatures for the source and the sink; however, the thermodynamic work accomplished per repetitive cycle of the ideal Carnot engine is relatively small. Thus, the efficiency of a Carnot engine as determined on the basis of shaft work produced can be severely degraded by even moderate mechanical inefficiencies. The thermodynamic work per cycle produced by the ideal Stirling engine is relatively much larger than that produced by the ideal Carnot engine; however, because the gas dynamic and mechanical friction losses in any practical Stirling engine are considerable, the shaft work per cycle produced by a practical Stirling engine must be appreciably lower than that predicted for the corresponding ideal Stirling engine.

In order to obtain a high specific power, i.e., a high power per unit volume displacement, the thermodynamic processes employed by any heat engine must be carried out rapidly. This necessity virtually always leads to thermodynamic irreversibilities and a resultant reduction in engine efficiency. A high source temperature is desirable, not only because the Carnot efficiency is increased by increasing this temperature, but because the transport processes within the normally gaseous or vaporous thermodynamic medium are enhanced at higher temperature.

One reason for the widespread utilization of Otto- and Diesel-cycle engines has been that these are cyclic internal combustion engines in which the effective thermodynamic source temperature is quite high while the temporal mean temperature of the boundaries within the combustion chamber can be maintained at a level that can be tolerated by the materials constituting the boundaries. On the other hand, development of the steady-flow Brayton-cycle engine was delayed until fairly recently by the unavailability of materials that could withstand the source temperature required for reasonably efficient operation of the engine.

Another reason for the predominance of Otto- and Diesel-cycle engines is that, because these are internal combustion engines, the heat added to the working medium is generated within the working space and does not have to be transferred through the solid boundary of the working space as is required in an external combustion engine.

Because the Stirling engine is an external combustion engine, the following is true:

(1) All of the heat entering the thermodynamic working space must be transferred through the heater tubes at a temperature at least slightly above the source temperature of the cycle.

(2) That part of the boundary at the high-temperature end of the working space within the engine must operate continuously at approximately the cycle source temperature and at a mean pressure of 50 to 150 atmospheres.

(3) All of the thermal energy transferred into the thermodynamic medium and not converted to work or lost by leakage through the boundaries must be rejected through the engine coolers. While this last requirement does not impose serious materials problems on the design of the Stirling engine, it does necessitate a heat rejection system possessing as much as three times the cooling capacity of the heat rejection system associated with an Otto- or Diesel-cycle engine of the same power rating operating between the same temperatures of source and sink.

# SECTION III

## ATTRACTIVE CHARACTERISTICS OF THE STIRLING ENGINE

The following characteristics of the Stirling-cycle engine make it an attractive candidate for solar thermal electric applications:

(1) High thermal efficiency: The relatively high thermal efficiency of the Stirling engine is indicated by Figure 2-11. Even higher efficiencies appear possible if isothermalizers, low-drag regenerators, and hydrostatic bearings and seals can be successfully incorporated into a carefully designed Stirling engine.

(2) Dynamically balanced, valveless, closed-cycle operation: Many dynamically balanced Stirling engines, kinematic and free-piston, single and multiple cylinder, have been designed. There is scarcely a reason for considering a Stirling engine that is not dynamically balanced. Therefore, mechanical vibration of the engine assembly is minimal.

Because the Stirling engine is valveless and, in the case of the solar-powered engine, has no intake from or exhaust to the ambient air, engine operation can be expected to be far quieter than Otto- or Diesel-engine operation. Even when a fossil-fuel combustor is employed as the heat source for a Stirling engine, the continuous nature of the combustion process can be expected to allow the engine to operate more quietly and with less pollution than a comparable Otto or Diesel engine.

(3) Insensitivity of engine efficiency to engine size: Design analyses have indicated that little or no penalty in engine efficiency is incurred by Stirling engines of small size, e.g., one to twenty-five kilowatts output, as compared with large engines of up to two thousand kilowatts output (Ref. 11).

## SECTION IV

## STIRLING ENGINE DEVELOPMENT PROBLEMS

The following development problems have been identified for the Stirling engine:

(1) Regenerator effectiveness: A regenerator accepts thermal energy from a working fluid during one phase of the Stirling cycle and returns the energy during another phase.

Regenerator effectiveness is defined as,

$$E = \frac{T_R - T_C}{T_H - T_C} ; \tag{35}$$

when $E < 1$, engine efficiency is reduced.

In general terms, regenerator effectiveness increases and regenerator flow losses decrease with increasing regenerator void volume. Unfortunately, regenerator void volume is a part of the so-called dead volume of the engine, and increasing the dead volume reduces the pressure ratio and, hence, the performance of the engine.

(2) Dead space: Dead space is that part of the working space that is not swept by the pistons. Stirling engine dead space includes:

(a) Hot-end cylinder clearance volume

(b) Heater internal volume

(c) Regenerator void volume

(d) Cooler internal volume

(e) Cold-end cylinder clearance volume

(f) Connecting duct volumes

Foreseeable improvements in conventional Stirling engine design cannot reduce dead space below about one-half the minimum total working space volume.

Dead space reduces work output per cycle, even with perfect regeneration.

Based on first- and second-order analyses, dead space reduces engine efficiency even when regeneration is perfect.

(3) Expansion and compression processes are more nearly adiabatic than isothermal: Each of the primary volumes wherein the expansion and compression processes take place in the Stirling engine is enclosed by the cylinder end walls and the piston end. In conventional designs, the surface available for heat transfer to or from the enclosed gaseous medium is limited. Furthermore, at the usual cyclic rate of the engine, the distance from the enclosing surface into the gas to which the heating or cooling of the solid surface exerts any appreciable effect on the temperature of the medium is also severely limited. Thus, in conventional designs, the expansion and compression processes are much more nearly adiabatic than isothermal, and isothermal expansion and compression are required for ideal Stirling engine operation.

In recent years, attempts have been made to design the expansion and compression spaces so as to make the thermodynamic processes occurring therein more nearly isothermal. The cylinder and piston ends have been fitted with mating sets of plane or axially symmetric interleaving fins comprising deep serrations or parallel plates. These so-called isothermalizers increase surface area and decrease the average distance of the medium from the bounding surface; thus, the concept rests on well established principles of heat transfer. It seems surprising that the concept has not been more thoroughly tested or more widely applied. This is even more surprising when one realizes that the application of isothermalizers within the working space, coupled with condensing liquid metal heat transfer from the source at the hot end of the engine and of boiling heat transfer to the sink at the cold end of the engine, would allow reduction, and perhaps even elimination, of the dead volumes associated with the heater and cooler of the conventional design. Direct radiation of energy through a window into the hot end of the engine has also been suggested.

(4) Stirling engine piston rings: Rings must operate in a hot, dry environment. The best currently used rings employ a teflon-filled inorganic matrix. Successful operation is measured in hundreds of hours. Higher-than-current operating source temperatures ( $>1350^{o}F$) will aggravate this problem. A gas bearing type of piston support and seal in the cylinder may be the best solution. However, two possible problems remain.

(a) Low friction in the gas bearing implies a large clearance and large pumping losses, while small clearance in the gas bearing implies smaller pumping losses but higher piston friction losses. In contemporary gas bearings, the pumping losses predominate (Ref. 12).

(b) The very close fit required for a satisfactory gas bearing complicates the problem of maintaining the correct clearance as the two mating parts heat and cool in transient operation and/or assume different temperatures in steady operation.

While the analogy is not perfect, it is sobering to consider the fact that, after more than fifty years of continuous development, properly lubricated, hard chrome rings in nitrided cylinder liners allow only about fifteen thousand hours of Diesel engine operation before overhaul or replacement is required.

(5) Piston rod seals: At least until very recently, the best Stirling engine rod seals have had an average operating life of a few hundred hours. This has been the most serious and stubborn operational problem of the modern kinematic Stirling engine.

Rod seals must limit leakage of the working fluid from the work space to avoid frequent recharging of the engine. Tight sliding seals mean large friction losses. Rolling seals have exhibited a very inconsistent and, on the average, a very limited fatigue life. Rod seals must prevent any lubricant other than the working fluid from migrating into the work space because oil entering the working space is quickly pyrolyzed and deposited on the regenerators, severely reducing engine efficiency. When hydrogen is employed as a working fluid, some of any oil entering the working space reacts with the hydrogen to form methane, this admixing of methane with the hydrogen also reduces engine efficiency.

As with the piston ring problem, a suitable gas bearing may provide a satisfactory solution -- at least for the free-piston-type engine.

(6) Materials strengths at the high source temperatures and high mean pressure in the working volume: Even at the heater tube and heater head design temperatures that have been commonly employed in contemporary Stirling engines, viz., approximately 1350°F, failure of heater tubes and/or heater heads due to elevated-temperature creep or combined mechanical and thermal stresses occur occasionally.

At the 1500°F to 1600°F source design temperatures anticipated for the metallic engines now being developed and tested, these types of materials failures will continue to be a serious problem, even when the heater tubes and head are fabricated from expensive, predominantly non-ferrous, high-temperature alloys.

At least one recently constructed prototype engine employed ceramic inserts in the heater head as a means for partially insulating the structural metallic head from the high-temperature medium. Currently, considerable interest is centered on the fabrication of complete heater tube and heater head assemblies from structural silicon carbide and/or silicon nitride. However, development of the techniques for constructing consistently sound subassemblies of these materials in a manner that will allow them to withstand high pressures, high temperatures, and large thermal transients has only begun.

(7) Mechanical efficiency: The mechanical efficiency of the kinematic-type Stirling is seldom more than 85% and is usually 80% or less if a rhombic drive is employed. The mechanical efficiency of the free-piston-type Stirling is hardly more than 90% because of gas bearing and gas spring losses, and the relatively low linear alternator efficiency demonstrated to date ($\leq 93\%$) will offset the relatively higher mechanical efficiency of the free-piston engine unless linear alternator efficiency can be improved considerably in future designs.

Friction losses in the piston and piston rod seals probably cannot be reduced very much unless hydrostatic sealing proves feasible. Similarly, piston pin friction and, in the case of the rhombic-drive kinematic engine, friction in the linkage pins that do not rotate continuously in one direction are probably irreducible unless hydrostatic bearings can be used in these locations.

(8) Cooling system: The Stirling engine is an external combustion engine; thus, all heat entering the working space must be converted to work, removed by the cooling system, or leak to the surroundings. Of course, indiscriminate heat leakage must be limited in order to insure efficient operation, while the energy converted to work is limited by Carnot's principle; the remaining energy -- roughly one-third to two-thirds of that supplied -- must be removed by the cooling system. As a result, the required cooling system capacity for a typical current Stirling engine is roughly three times that of a current Otto or Diesel engine of equal power output.

(9) The working medium: In order to provide high thermal capacity and high heat transport capability while, at the same time, incurring low turbulent flow losses, a low-density thermodynamic medium should be employed in an efficient Stirling engine. Hydrogen and helium are the two commonly used media. However, some concomitant problems are incurred with either of these choices. In any case, the mean working pressure in the usual Stirling engine is fifty to one hundred and fifty atmospheres, so an abrupt and potentially dangerous decompression is always possible except when the medium is withdrawn from the engine.

Because the molecular weight of either hydrogen or helium is low, leakage of the medium from the working space is a problem unless hermetic sealing of the engine-generator assembly can be accomplished. Even then, hydrogen can diffuse through hot metal parts. This task appears now to be less formidable in the case of the free-piston Stirling engine than in the case of the kinematic Stirling engine.

While the molecular weight of helium is approximately twice that of hydrogen, helium is monatomic while hydrogen is diatomic. Reference to Section II.B.2., "Regenerative Stirling Cycle with Regenerator Dead Space," allows the conclusion that, unless

regeneration is perfect, the efficiency of this cycle will increase with increasing ratio of specific heats, k. Because $k = 1.67$ for a monatomic gas while $k \approx 1.40$ for a diatomic gas at the temperatures to be encountered in metallic Stirling engines, helium is to be preferred on this basis. On the other hand, given identical operating conditions, the flow losses can be expected to be higher when helium rather than hydrogen is employed as the medium. Two additional problems should be noted: Hydrogen is highly flammable, and helium, while non-flammable, is only available in limited quantities and at a higher cost.

Consideration of some of the hazards noted above strongly indicates that skilled mechanical technicians -- equivalent in training and experience to licensed aircraft and engine mechanics -- will be required for the satisfactory maintenance of Stirling engines.

## SECTION V

## SUMMARY AND CONCLUSIONS

The major conclusions of this investigation support and reinforce the already widely held opinion that the Stirling engine is strongly competitive both technically and economically as the power conversion subsystem of an advanced point-focusing distributed receiver solar thermal power system.

In both magnitude and trend, brake efficiencies projected here are in satisfactory agreement with those estimated by United Stirling for advanced derivatives of their current P-40 and P-75 engines, e.g., a brake efficiency of forty percent (perhaps even one or two percent higher) at a heater head temperature of 1500°F and a cooler temperature of 140°F. Although the thermal efficiency of some current Stirling engines is quite high -- superior to virtually any other practical engine operating in the same temperature range -- considerably higher efficiency is promised by such developing innovations in Stirling engine design as isothermalizers, high-heat-transfer, low-flow-loss heat exchangers, and hydrostatic seals and bearings. Minimization of working space dead volume is a key to high Stirling engine efficiency; therefore, it is imperative that the hot-end, regenerator, and cold-end dead volumes be minimized. Another key to high engine efficiency is the highest regenerator effectiveness consistent with the concomitant requirements of minimum regenerator void volume and low flow loss. Regenerator effectiveness becomes increasingly important as the ratio of heater head temperature to cooler temperature is increased; thus, higher heater head temperature implies more precise regenerator optimization if engine efficiency is to be increased.

The Stirling engine appears to be well matched with the cavity receivers used in point-focusing distributed receivers in that highest combined efficiency appears to occur at no more than 1900°F, and this efficiency is only modestly reduced at receiver temperatures as low as 1600°F (Ref. 13). Of current major concern are the practical problems associated with assuring reliable, low-maintenance, long-life operation of practical Stirling engines that are cost-competitive with other engines, e.g., the gas turbine engine. The necessity for reducing or eliminating the use of expensive, high-temperature metal alloys that require strategically vulnerable alloying elements in Stirling engines is also clear but somewhat less pressing. If the durability, reliability, and serviceability of the kinematic Stirling engine is to be improved appreciably, the durability, reliability, and serviceability of piston rod seals, piston rings, and heater heads must be greatly improved. Therefore, it appears that, at least until considerable improvement is assured, advanced technological development activities should be concentrated on these components.

While the promise that appears to be offered by properly designed advanced free-piston Stirling engines has been only outlined in this report, that promise should be the object of further investigation.

## REFERENCES


1. Fortgang, H. R., "Cost Estimating Brayton and Stirling Engines," Proc. First Semiannual Distributed Receiver Systems Program Review, held in Lubbock, Texas, January 22-24, 1984, (DOE/JPL-1060-33, JPL Publication 80-10, April 15, 1980).

2. Fujita, T., El Gabalawi, N., Herrera, G., and Turner, R. H., Projection of Distributed-Collector Solar Thermal Electric Power Plant Economics to Years 1990-2000, DOE/JPL-1060-77/1 (JPL Publication 77-79), December 1977.

3. Fujita, T., Manvi, R., Roschke, E. J., El Gabalawi, N., Herrera, G., Kuo, T. J., and Chen, K. H., Techno-Economic Projections for Advanced Small Solar Thermal Electric Power Plants to Years 1990-2000, DOE/JPL-1070-4 (JPL Publication 79-25), November 15, 1978.

4. Latta, A. F., Bowyer, J. M., Fujita, T., and Richter, P. H., The Effects of Regional Insolation Differences Upon Advanced Solar Thermal Electric Power Plant Performance and Energy Costs, DOE/JPL-1060-17 (JPL Publication 79-39), March 15, 1979; paper also published in J. Solar Energy Engineering, Vol. 103, pp. 213-220, August 1981.

5. Advanced Subsystems Development Second Semiannual Progress Report, April 1, 1978 to October 1, 1978, DOE/JPL-1070-7 (JPL Publication 79-24), November 15, 1978.

6. Martini, W. R., Stirling Engine Design Manual, DOE/NASA/3152-81, NASA CR-135382, April 1978.

7. H. Hausen, "Vervollständigte Berechnung des Wärmeaustausches in Regeneratoren," Z.VDI, Vol. 2., pp. 31-44, 1942.

8. Communication from David M. Berchowitz, Mechanical Technology, Inc., Latham, New York 12110, which included Appendix A "The Ideal Second Order Stirling Cycle (Schmidt)" from a late draft of his doctoral thesis.

9. Walker, G., "Elementary Design Guidelines for Stirling Engines," Proc. 14th IECEC, Boston, Massachusetts, August 5-10, 1979, Vol. 1, published by American Chemical Society, 1155 Sixteenth Street, N.W., Washington, D. C. 20036.

10. Tew, R., Jefferies, K., Miao, D., A Stirling Engine Computer Model for Performance Calculations, DOE/NASA/1011-78/24, NASA TM-78884, July 1978.

11. Hoagland, L. C., and Percival, W. H., "Potential of the Stirling Engine for Stationary Power Applications in the 500-2000 HP Range," Proc. 13th IECEC, Vol. 3, pp. 1865-1871, 1979, published by Society of Automotive Engineers, Inc., Warrendale, Pennsylvania, 15096.

12. Rieger, N. F. (design note editor), Design of Gas Bearings 1967, notes supplemental to the RPI-MTI course on gas bearing design, August 14-17, 1967, Vols. I and II, published by Rensselaer Polytechnic Institute and Mechanical Technology, Inc.

13. Fujita, T., Bowyer, J. M., and Gajanana, B. C., "Comparison of Advanced Engines for Parabolic Dish Solar Thermal Power Plants," Journal of Energy, Vol. 6, No. 5, pp. 293-297, September-October 1982.

APPENDIX

# REFINED CALCULATION OF THE HEAT EXCHANGE IN REGENERATORS [0]*

by H. Hausen

(Translated by J. M. Bowyer)

A theory of heat exchange in primarily ceramic regenerators is extended in such a way that even the rapid temperature changes immediately following the flow reversals and the deviations in temperature gradients at the ends of the regenerator can be considered. The equations and diagrams presented allow an exact calculation of regenerators, even under unusual conditions, and apply even in the limiting cases of arbitrarily thin or thick ceramics.

In the language of the smelting industry, a regenerator is understood to be a reversible flow heat exchanger through which gas flows alternately in opposite directions and in which a mass of large thermal capacity periodically accepts and rejects the thermal energy that passes through it.

In the case of ceramic regenerators operating at high temperature, e.g., the air preheater of a blast furnace, the heat exchange achieved depends, among other things, on the temperature variation within a cross section of the ceramic. On the basis of these temperature variations, Heiligenstaedt [1] and Rummel [2] have formulated equations for the calculation of a regenerator heat exchange coefficient or, respectively, a regenerator heat transfer coefficient. Heiligenstaedt [3] proceeded from the simplifying assumption that the gas temperatures do not vary with time; Rummel proceeded, in part, from empirical expressions. The author [4] has derived an equation that is based purely on theory and yet is simple and better fitted to the actual behavior (of a regenerator). However, as already emphasized in the (earlier) publication [4], calculation still neglects certain very rapid temperature changes which appear immediately after each flow reversal. Under the circumstances, even the deviating temperature gradient at the ends of the regenerator required a separate calculation for which a fully developed method was indicated at the conclusion of the report [5]. Under ordinary conditions the two effects mentioned (above) are usually small. However, in order to be able to consider them consistently correctly and yet quickly, an extended theory [6] is developed in what follows. In this way, it is possible to calculate very precisely the temperature gradient at all locations in a regenerator, as well as the heat transfer coefficient, even under unusual conditions.

---

*Numbers in brackets represent Notes at the end of the Appendix.

## Fundamental Concepts of the Previously Developed Theory

The following investigations follow directly from the previously developed, simpler theory. Therefore, the basic concepts and the results of this (simpler) theory will be briefly discussed. We consider the temperature variation within a cross section of the ceramic that is perpendicular to the direction of flow of the gases (Figure A-1)*. To distinguish clearly, let the ceramic temperatures be denoted by $\tau$, the temperature of the warmer gas by $\theta$, and that of the cooler gas by $\theta'$. Because the outer surface of the ceramic is washed alternately by warmer and cooler gas, the ceramic temperature, $\tau$, oscillates constantly up and down between the two limits $\tau_{max}$ and $\tau_{min}$. These oscillations are larger near the outside surface than they are in the interior of the ceramic. How the oscillations under particular conditions proceed depends on the way in which the gas temperatures, $\theta$ and $\theta'$, vary with time.

On the basis of experimental results as well as on theoretical considerations concerning low-temperature regenerators, the simpler theory assumed that the gas temperatures at the cross section of interest varied linearly with time between each two successive flow reversals. With the help of the finite difference method of Binder and Schmidt [7], one can then obtain the approximate (spatial) temperature profiles at various fixed times as shown in Figure A-2. The figure shows the cooling of a 40-mm-thick ceramic during the cooling period, that is, during the time in which the cooler gas flows through the regenerator. The duration of this period, as well as (that) of the subsequent heating period, has been assumed to be 12.75 min.

At the start of the cooling period, the temperature distribution, which was obtained from a separate consideration of the steady (oscillating) state, is represented by a parabola or parabolic curve that is concave upward. As a result of the initially very rapid cooling of the outer layers of the ceramic, this curve is deformed and, after about three minutes, is transformed into a parabola that is concave downward. Subsequently, the curve moves downward with unchanging form and constant speed.

If one plots this temperature variation as a function of time and, indeed, for cooling and heating periods whose times are measured in opposite directions, one obtains Figure A-3. The dashed lines represent the gas temperatures, and the solid, closed line, the outside surface temperatures, $\tau_o$ and $\tau_o'$, of the ceramic during the heating and cooling periods. At other locations in the ceramic, the temperatures traverse closed lines but with smaller vertical amplitude. However, if one determines a local mean value for the temperature $\tau_m$ or $\tau_m'$ of the ceramic across the entire width of the cross section by application of the approximate method at each instant, one is led to the remarkable result that the temporal variation of this mean value can be very well represented by a single straight line which is

*Figures appear at the end of the Appendix following Notes.

traversed in opposite directions in the two periods (heating and cooling). This encompasses a further, more general perception. If the times of the two periods which, in the chosen representation, assume the same abscissa are called "mutually corresponding times," then for such times, corresponding to Figure A-3,

$$\tau_m = \tau_m'. \tag{1}$$

Figure A-3 shows furthermore that, aside from the very rapid temperature changes immediately after the flow reversal, even the outer surface temperatures $\tau_o$ and $\tau_o'$ vary linearly during most of each period. Therefore, the assumption was made in the earlier theory that all temperatures in the ceramic varied with time in a completely linear way, as is illustrated in Figure A-4. On the basis of this assumption, a purely parabolic temperature distribution was obtained from the differential equation for heat conduction. Using Equation (1), this temperature distribution ultimately led to a relationship for the heat transfer coefficient for which K. Rummel [8] has introduced the following definition. Let T be the duration of the heating period and T' that of the cooling period. Then the heat transfer coefficient, k, is defined as the quantity of thermal energy accepted and then rejected by one $m^2$ of the regenerator heating surface in a complete period, T + T', divided by the temporal mean value of the temperature difference, $\theta - \theta'$, between the warm and cool gases. The relationship for k derived on the basis of the completely linear variation of temperature with time is

$$\frac{1}{k} = (T + T') \left[ \frac{1}{\alpha T} + \frac{1}{\alpha' T'} + \left( \frac{1}{T} + \frac{1}{T'} \right) \frac{\delta}{6\lambda} \right] \tag{2}$$

where $\alpha$ and $\alpha'$ represent the thermal conductances during the warm and cool periods, and $\delta$ and $\lambda$ represent the thickness and thermal conductivity of the ceramic. Accordingly, the quantity of heat transferred from the entire heat transfer surface, F, in one complete period, T + T', is

$$Q = kF\ (T + T')\ (\theta - \theta')_M\ , \tag{3}$$

where $(\theta - \theta')_M$ represents the mean temperature difference between the two gases and k has the same value at all points within the regenerator.

## The Differential Equations for Heat Exchange in the Regenerator as the Basis of the Extended Theory

The neglected (factors) of the previously developed theory that were mentioned in the introduction can now be more precisely identified. As shown in Figure A-3, not only at the outer surfaces, but also within the ceramic,

very rapid temperature changes occur immediately following the flow reversal. However, sooner or later these variations tend toward the linear variation of temperature with time. These rapid temperature changes, hitherto neglected, cause a larger error the thicker the ceramic elements and the shorter the duration of the heating and cooling periods are. Furthermore, as a rule, the assumption of a completely linear distribution of the mean ceramic temperatures, $\tau_m$ and $\tau_m'$ , as well as the relationship $\tau_m = \tau_m'$ for the mutually corresponding times of the two periods is very well justified in the large middle part of the regenerator. However, it is no longer valid at the ends of the regenerator where the variations of $\tau_m$ and $\tau_m'$ are nonlinear and, as should be indicated more precisely, are bent, forming a hysteresis loop, vide Figure A-20.

Now, in order to develop a theory that accounts for these two deviations numerically, we will consider all of the periodic temperature variations in the steady operation of the regenerator as induced temperature oscillations. We will analyze these oscillations in a manner similar to that (employed in analyzing) the fundamental and higher harmonic vibrations of a string. It will then become apparent that an exact calculation of the fundamental oscillation will enable formulation of the rapid temperature variations following the flow reversal. In contrast, it will only be possible to calculate the temperature deviation at the end of the regenerator by including the harmonics. The applicable equations for the fundamental and harmonic oscillations can be obtained from the differential equations governing heat exchange in the regenerator. Therefore, these differential equations should next be briefly discussed.

The heat conduction equation is valid for the temperature changes inside a cross section of ceramic that is perpendicular to the direction of flow:

$$\left(\frac{\partial \tau}{\partial t}\right)_y = a \left(\frac{\partial^2 \tau}{\partial y^2}\right)_t , \tag{4}$$

where $\tau$ represents the temperature of the ceramic at distance y from its left-side, outer surface (cf. Figure A-2), t the time, and $a = \lambda/(\gamma c)$ the thermal diffusivity. In turn, $\lambda$ represents the thermal conductivity of the ceramic (as noted earlier), $\gamma$ its density, and c its specific heat. In Equation (4), the thermal conductance of the ceramic in the streamwise direction is neglected as unimportant [9].

Henceforth, let f be the heat transfer surface of the ceramic (elements) measured from the entrance point of the gas into the regenerator up to the cross section of interest, and let W be the thermal capacity of the gas flowing through the regenerator per unit time during the heating part of the cycle. As is easily determined, the following two differential equations for heat exchange in the regenerator are then valid:

$$\left(\frac{\partial \theta}{\partial f}\right)_t = \frac{\alpha}{W} (\tau_o - \theta) \tag{5}$$

and

$$\left(\frac{\partial \tau_m}{\partial t}\right)_f = \frac{2\alpha}{\gamma c \delta} (\theta - \tau_o). \qquad (6)$$

The meaning of these equations is immediately clear if one multiplies Equation (5) by -W and Equation (6) by $\gamma c\delta/2$, which represents the thermal capacity per unit area of the heated surface of the ceramic (considered to be a flat surface).

Thus, Equation (5) expresses the fact that heat given up by the passing gas to unit surface area of the ceramic per unit time is equal to the heat transferred between the gas and the surface of the ceramic through the temperature difference $\theta - \tau_o$. Equation (6) states that the same quantity of heat is transferred from the gas to the regenerator (represented by the right member of Equation (5) multiplied by W) and, in consequence, the mean temperature of the ceramic, $\tau_m$, increases by $(\partial\tau_m/\partial t)_f$ per unit time. Equations (5) and (6) also apply to the cooling periods if $\theta$, $\tau_o$, $\tau_m$, $\alpha$, and W are replaced by $\theta'$, $\tau_o'$, $\tau_m'$, $\alpha'$, and W' and if heat transferred from the ceramic surface to the gas is now counted as positive.

In order to find solutions of these equations which describe the steady state of the regenerator, the further condition must be fulfilled. At the end of a complete cycle consisting of a heating and a cooling period, the temperature at every point in the ceramic must be the same as it was at the start of that cycle. This condition is called the flow reversal condition. There are infinitely many solutions which satisfy this condition. These are the eigenfunctions, and, at times, are indicated by an "eigenvalue," $\kappa$, which may be any integer of the infinite series that extends from 0 to $\infty$.

As will be shown, the eigenfunction for $\kappa = 0$ represents the fundamental oscillation, while the higher eigenfunctions $\kappa \geq 1$ yield the harmonics.

For simplicity, only the eigenfunctions for the case that the heat capacities of the two gases streaming through the regenerator are temperature-independent and the durations of the heating and cooling periods are equal will be discussed. If, as earlier, W and W' represent the heat capacities of the gases per unit temperature, and T and T', the duration of the heating and cooling periods, this (the foregoing limitation on eigenfunctions) means we will limit ourselves to the case WT = W'T'. However, it will be briefly indicated in conclusion that the results of these considerations remain applicable and sufficiently accurate, even in general cases.

## The Fundamental Oscillation (Zeroth Eigenvalue)

In most earlier works regarding the calculation of ceramic regenerators, it was assumed as obvious that the temperatures in the lengthwise direction of a regenerator varied just as they do in a recuperator, i.e., as in steady flow through a tubular heat exchanger. In this analogy, the temperature distribution in the regenerator is considered at a definite time or at a time corresponding to the middle of a (heating or cooling) period. Among the known solutions of the differential equations, one can always be found that

represents this simplest longitudinal temperature distribution, and it can be demonstrated that this solution is obviously the zeroth eigenfunction ($\kappa = 0$) that corresponds to the fundamental oscillation [10]. Thus, the zeroth eigenfunction can also be defined as that which yields the same longitudinal temperature distribution (in the regenerator) as is found in a recuperator. Then if, hereafter, we seek the zeroth eigenfunction for (the case) WT = W'T', we must, for the analogy, refer to a recuperator in which the thermal capacities of the two gases are likewise equal. It is known that, in this case, a completely linear temperature distribution is established in the recuperator as long as W, W', $\alpha$, and $\alpha'$ are constant, cf. Figure A-5. Therefore, the zeroth eigenfunction must present, at every instant, a linear temperature distribution in the longitudinal direction of the recuperator. Because the longitudinal coordinate was chosen to be the heat transfer surface, f, extending up to the cross section of interest, hereafter

$$\left(\frac{\partial\theta}{\partial f}\right)_t = \left(\frac{\partial\tau}{\partial f}\right)_t = \left(\frac{\partial\tau_m}{\partial f}\right)_t = \text{constant} \tag{7}$$

will be valid for the gas temperature, $\theta$, as well as for the temperature of the ceramic, $\tau$, at any particular time, t.

Equation (7) immediately allows important conclusions to be drawn from the differential equations if, beside $\alpha$ and W, the parameters $\lambda$, $\gamma$, c, and $\delta$ are also assumed constant. First, from Equation (5), it follows that $\tau_o - \theta$ = constant, that is to say, the temperature difference between the outer surface of the ceramic and the gas remains constant during the entire (heating or cooling) period. Furthermore, from Equation (6) we obtain

$$\left(\frac{\partial\tau_m}{\partial t}\right)_f = \text{constant}. \tag{8}$$

From the linear variation (of $\tau_m$) in the longitudinal direction [and Equation (8)], it follows that the mean temperature of the ceramic at each cross section varies linearly with time. This rule that was viewed earlier as only a very good approximation is thus proved to be an exact requirement of the zeroth eigenfunction when WT = W'T'. Consequently, for mutually corresponding times of the two periods, Equation (1),

$$\tau_m = \tau_m' , \tag{1}$$

is exactly satisfied by the zeroth eigenfunction. Recognizing this, the mean temperatures of the ceramic, $\tau_m$ and $\tau_m'$, become of fundamental importance to further considerations. Certainly, they form a simple framework upon which the essentially complicated behavior of the individual temperatures of the ceramic, $\tau$ and $\tau'$, and the gas temperatures, $\theta$ and $\theta'$ will be constructed.

## The Temperature Behavior According to the Zeroth Eigenfunction

Figures A-2 and A-3 already provide an approximate demonstration as to how the gas temperatures and ceramic temperatures behave when restricted to the zeroth eigenfunction. In order to be able to calculate exactly the temperature behavior under widely different conditions, we employ the following solution of the differential equation [Equation (4)]:

$$\tau = C + \left(\frac{\partial \tau_m}{\partial t}\right)_f \cdot t - \frac{1}{2a}\left(\frac{\partial \tau_m}{\partial t}\right)_f y(\delta - y) + \sum_{n=1}^{\infty} B_n \cdot e^{-\beta_n^2 at} \cos \beta_n \left(y - \frac{\delta}{2}\right) \quad (9)$$

where C, $B_n$, and $\beta_n$ represent initially arbitrarily chosen constants and $(\partial \tau_m/\partial t)_f$ is invariant in consequence of Equation (8). The lower case letter n represents a positive integer. The first term following C expresses the fact that $\tau_m$ should vary linearly with time. The second term presents the parabolic temperature distribution as it tends to develop toward the end of the period, cf. Figure A-2, A-7, or A-18. The last term, involving the cosine, yields the deviations from the parabolic distribution which are important immediately after the flow direction is reversed. Incidentally, because this member is a function of y, it is inferred that the solution must be symmetric with respect to the center of the ceramic, $y = \delta/2$.

In order to maintain the linear behavior of $\tau_m$, we determine the values of $\beta_n$ so that the mean value evaluated over the entire thickness of the ceramic, $\delta$, causes every cosine term to disappear; thus, these members make no contribution to $\tau_m$. Therefore, we set

$$\frac{1}{\delta}\int_o^{\delta} \cos \beta_n \left(y - \frac{\delta}{2}\right) dy = 0$$

and thereby obtain

$$\beta_n = \frac{2n\pi}{\delta} . \quad (10)$$

Similarly, the mean value of the parabolic term disappears if $\delta^2/6$ is subtracted from $y(\delta - y)$. Because it is still possible arbitrarily to choose the sign of $B_n$ by considering Equations (6) and (10), Equation (9) can also be written as

$$\tau = \tau_m - \frac{\alpha}{\lambda\delta} (\theta - \tau_o) \left[ y (\delta - y) - \frac{\delta^2}{6} \right]$$

$$+ \sum_{n=1}^{\infty} B_n \, e^{-\left(\frac{2n\pi}{\delta}\right)^2 at} \cos \left(2n\pi \frac{y}{\delta}\right) \quad . \tag{11}$$

We associate this equation with the heating period; correspondingly, for the cooling period we obtain

$$\tau' = \tau_m' - \frac{\alpha'}{\lambda\delta} (\theta' - \tau_o') \left[ y (\delta - y) - \frac{\delta^2}{6} \right]$$

$$+ \sum_{n=1}^{\infty} B_n' \, e^{-\left(\frac{2n\pi}{\delta}\right)^2 at'} \cos \left(2n\pi \frac{y}{\delta}\right) \quad . \tag{12}$$

We can further transform the last equation if we consider that, per unit surface area, the same quantity of heat, q, is exchanged in the cooling period as is exchange in the heating period. Thus,

$$q = \alpha' (\tau_o' - \theta') T' = \alpha (\theta - \tau_o) T \tag{13}$$

applies, and, thus, Equation (12) is transformed into

$$\tau' = \tau_m' + \frac{\alpha}{\lambda\delta} (\theta - \tau_o) \frac{T}{T'} \left[ y (\delta - y) - \frac{\delta^2}{6} \right]$$

$$+ \sum_{n=1}^{\infty} B_n' \, e^{-\left(\frac{2n\pi}{\delta}\right)^2 at'} \cos \left(2n\pi \frac{y}{\delta}\right) \quad . \tag{14}$$

In each period, the time t or t' should be redefined as zero at the instant flow reversal begins.

The values of $B_n$ and $B_n'$ are obtained from the flow reversal condition whereby the ceramic temperature, $\tau$, at the beginning of the heating period should have the same value as at the end of the cooling period, $\tau'$, and vice versa. If we determine the temperature at the start of the heating period (t = 0) from Equation (11) and the temperature at the end of the cooling period (t' = T') from Equation (14), then equating (these two equations) and recalling Equation (1),

$$\sum_{n=1}^{\infty} \left[ B_n - B_n' \, e^{-\left(\frac{2n\pi}{\delta}\right)^2 aT'} \right] \cos\left(2n\pi \, \frac{y}{\delta}\right) = \frac{\alpha}{\lambda\delta} (\theta - \tau_o)\left(1 + \frac{T}{T'}\right)\left[y\,(\delta - y) - \frac{\delta^2}{6}\right]. \tag{15}$$

On the left side of this equation is a Fourier series with the yet-to-be-determined coefficients,

$$B_n - B_n' \, e^{-\left(\frac{2n\pi}{\delta}\right)^2 aT'} .$$

If the right side of Equation (15) is defined as f(y), then according to the known formula for determining the Fourier coefficients,

$$B_n - B_n' \, e^{-\left(\frac{2n\pi}{\delta}\right)^2 aT'} = \frac{2}{\delta} \int_o^{\delta} f(y) \cos\left(2n\pi \, \frac{y}{\delta}\right) dy,$$

and, performing the integration,

$$B_n - B_n' \, e^{-\left(\frac{2\pi n}{\delta}\right)^2 aT'} = - \frac{1}{(n\pi)^2} \frac{\alpha\delta}{\lambda} (\theta - \tau_o) \frac{T + T'}{T} . \tag{16}$$

A similar consideration of conditions at the end of the heating period and the beginning of the cooling period yields

$$B_n' - B_n \, e^{-\left(\frac{2n\pi}{\delta}\right)^2 aT} = + \frac{1}{(n\pi)^2} \frac{\alpha\delta}{\lambda} (\theta - \tau_o) \frac{T + T'}{T} . \tag{17}$$

If Equations (16) and (17) are solved for $B_n$ and $B_n'$ and then $B_n$ is substituted into Equation (11), the most general form of the zeroth eigenfunction for WT = WT' is

$$\tau = \tau_m - \frac{\alpha\delta}{\lambda}(\theta - \tau_o)\left[\frac{y}{\delta}\left(1 - \frac{y}{\delta}\right) - \frac{1}{6} + \frac{T + T'}{T'}\right.$$

$$\left. \cdot \sum_{n=1}^{\infty} \frac{1 - e^{-\left(\frac{2n\pi}{\delta}\right)^2 aT'}}{1 - e^{-\left(\frac{2n\pi}{\delta}\right)^2 a(T+T')}} \cdot \frac{e^{-\left(\frac{2n\pi}{\delta}\right)^2 at} \cos\left(2n\pi \frac{y}{\delta}\right)}{(n\pi)^2}\right] . \qquad (18)$$

In the above equation, by comparison with Equation (6), $\tau_m$ is given by

$$\tau_m = \left(\tau_m\right)_a + \left(\frac{\partial \tau_m}{\partial t}\right)_f t = \left(\tau_m\right)_a + \frac{2\alpha}{\gamma c \delta}(\theta - \tau_o)t \ , \qquad (19)$$

where $(\tau_m)_a$ represents the value of $\tau_m$ at the start of the period. Using Equations (18) and (19), calculate the complete temperature behavior for the period of interest and, by a corresponding application (of the method) also calculate the complete temperature behavior in the immediately following period. The gas temperature $\theta$ is obtained from Equation (18) by calculating the ceramic surface temperature (y = 0) and adding it to the temporally invariant quantity $\theta - \tau_o$.

## Comparison of Theory with Experiment

Although the accuracy of the relationships found follows from the rigorous, exact derivation carried out (above), it furthermore may be shown that it is also confirmed by experiment. The temperature behavior calculated by Equations (18) and (19) in an 80-mm-thick ceramic, for which the period durations T = T' = 1 h are assumed and for WT = W'T', is shown in Figures A-6 and A-7. The curves in Figure A-6 give the temporal temperature distribution at a specified cross section of the ceramic at its outer surface (y = 0), at distances of 15 and 25 mm from the outer surface, and at its mid-plane (y = 40 mm). (See also Figure A-3.) The linear behavior of the mean temperatures of the ceramic, $\tau_m$ and $\tau_m'$, is indicated by the dot-dash

line. As in Figure A-2, Figure A-7 shows the temperature distribution in the ceramic's cross section at different times, t. For comparison with the curves in Figure A-6, the measurements of Schumacher [13] are presented in Figure A-8. The experimental regenerator has the same characteristics as those relating to Figure A-6. The agreement between calculation and experiment is, to the accuracy of the experiments, very good. In particular, it can be recognized that even the rapid temperature changes immediately following the flow reversal are correctly represented by the newly developed equations. The good agreement also extends to the temporal behavior of the gas temperatures, $\theta$ and $\theta'$; calculated results are shown in Figures A-9 through A-12, and the experimental results of Schumacher are shown in Figures A-13 through A-16. Also, in contrast to the assumptions imposed in Figure A-3, the temperature trend (presented) here is curved immediately after the flow reversal and becomes monotonically more nearly linear toward the end of the period. When comparing results, note that the measurements across an 80-mm-thick ceramic are presented in Figures A-13 through A-16 while the calculated curve in Figure A-12 corresponds to a 200-mm-thick ceramic. (Compare also Figures A-17 and A-18.)

How the temperature distribution in the ceramic varies if the ceramic is thicker or the period shorter should now be further explained. The thicker the ceramic, the longer the time (required) for transition from parabolic or quasi-parabolic curve concave upward to the concave downward form. For very thick ceramic this (transition) can require so much time that, even at the end of the period, the fully parabolic form is not completely achieved. Furthermore, the deviation from this form becomes larger as the period shortens. Figures A-17 and A-18 show the result of a precise calculation for a 200-mm-thick ceramic under otherwise identical conditions as (those imposed) in Figures A-6 and A-7 and where, in particular, the duration of a period is assumed to be 1 h. One recognizes that the middle (region) of the ceramic participates very little in the temperature oscillations and, for this reason, in the heat exchange. Assuming a constant time for the period, the temperature oscillations in the middle (region) of the ceramic are virtually non-existent beyond a certain thickness of the ceramic. A further increase in the thickness of the ceramic can then no longer affect the heat exchange. Because of this, the heat transfer coefficient must also be independent of ceramic thickness.

## The Heat Transfer Coefficient, $k_o$, Corresponding to the Zeroth Eigenfunction

Once the temperature behavior is determined from Equations (18) and (19), the heat transfer coefficient, $k_o$, that corresponds to the zeroth eigenfunction can be determined without special difficulty.

First, the temporal mean value of the ceramic's external surface temperature during the heating period, $(\tau_o)_M$, is determined by setting $y = 0$ in Equation (18) and integrating (the result) with respect to time, t, from 0 to T. Thus is obtained

$$(\tau_o)_M - (\tau_m)_M = \frac{\alpha\delta}{6\lambda}\,(\theta - \tau_o)\phi\ , \qquad (20)$$

where $(\tau_m)_M$ represents the temporal mean of $\tau_m$ and $\phi$ is an abbreviation for

$$\phi = 1 - 3\,\frac{\delta^2}{2a}\left(\frac{1}{T}+\frac{1}{T'}\right)\cdot\sum_{n=1}^{\infty}\frac{1}{(n\pi)^4}\,\frac{\left[1-e^{-\left(\frac{2n\pi}{\delta}\right)^2 aT}\right]\left[1-e^{-\left(\frac{2n\pi}{\delta}\right)^2 aT'}\right]}{1-e^{-\left(\frac{2n\pi}{\delta}\right)^2 a(T+T')}}\cdot \qquad (21)$$

In a similar way, for the cooling period,

$$(\tau_m')_M - (\tau_o')_M = \frac{\alpha\delta}{6\lambda}\,(\theta - \tau_o)\,\frac{T}{T'}\,\phi \qquad (22)$$

is obtained.

Now the temporal mean value, $(\theta - \theta')_M$, representing the difference of the gas temperatures, can be calculated with Equations (20) and (22). Because $\theta - \tau_o$ = constant, $\tau_o' - \theta'$ = constant, and $(\tau_m)_M = (\tau_m')_M$ [from Equation (1)], $(\theta - \theta')_M$ can be determined from

$$(\theta - \theta')_M = (\theta - \tau_o) + \left[(\tau_o)_M - (\tau_m)_M\right] + \left[(\tau_m')_M - (\tau_o')_m\right] + (\tau_o' - \theta'). \qquad (23)$$

By substituting Equations (20) and (22) into Equation (23), recalling Equation (13),

$$(\theta - \theta')_M = (\theta - \tau_o)\left[1 + \frac{\alpha T}{\alpha' T'} + \left(1 + \frac{T}{T'}\right)\frac{\alpha\delta}{6\lambda}\phi\right] \qquad (24)$$

is obtained.

From the definition of the heat transfer coefficient, for each $m^2$ of heating surface over a complete (regenerator) cycle, T + T', the quantity of heat, q [= Q/F, cf. Equation (3)], absorbed and again given up by the ceramic is

$$q = \alpha\,(\theta - \tau_o)\,T = k_o\,(\theta - \theta')_M\,(T + T'). \qquad (25)$$

From this (last equation), employing $(\theta - \theta')_M$ from Equation (24), the following formula for the heat transfer coefficient, $k_o$, is obtained:

$$\frac{1}{k_o} = (T + T')\left[\frac{1}{\alpha T} + \frac{1}{\alpha' T'} + \left(\frac{1}{T} + \frac{1}{T'}\right)\frac{\delta}{6\lambda}\,\phi\right] . \qquad (26)$$

This equation differs from the previously derived formula [Equation (2)] only by the appearance of the factor $\phi$. This factor expresses the effect of the very rapid temperature changes following flow reversal. While, as a result of neglecting this effect, the earlier equation was the more inaccurate the thicker the ceramic and the shorter the duration of the complete period, Equation (26) remains exact in the realm of solutions expressible by the zeroth eigenfunction for infinitely thick ceramic and for arbitrarily long durations of the period.

The appearance of the function $\phi$ [in Equation (26)], which can be determined from Equation (21), appears at first to make the calculation of $k_o$ unnecessarily difficult. However, it is possible to replace Equation (21) by the following very accurate approximate formulae:

$$\text{for} \quad \frac{\delta^2}{2a}\left(\frac{1}{T} + \frac{1}{T'}\right) \leq 10, \qquad \phi = 1 - \frac{1}{30}\frac{\delta^2}{2a}\left(\frac{1}{T} + \frac{1}{T'}\right); \qquad (27)$$

$$\text{for} \quad \frac{\delta^2}{2a}\left(\frac{1}{T} + \frac{1}{T'}\right) \geq 10, \qquad \phi = \frac{2.142}{\sqrt{0.3 + \frac{\delta^2}{2a}\left(\frac{1}{T} + \frac{1}{T'}\right)}} . \qquad (28)$$

It is even simpler to obtain $\phi$ from Figure A-19 wherein $\phi$ from Equation (21) is presented graphically as a function of $\delta^2/2T$ or, as the case may be, $(\delta^2/2a)\,(1/T + 1/T')$. The solid curve is valid for $T = T'$, while the dashed curves are valid for $T = 2T'$ or $T = 1/2\ T'$ or for $T = 4T'$ or $T = 1/4\ T'$. The dashed lines show that, even for $T = 4T'$ or $T = 1/4\ T'$, the deviations from the values for $T = T'$ are very small. Therefore, in almost all practical cases, it will be possible to determine $\phi$ with sufficient accuracy by means of the graph (of Figure A-19) or from Equations (27) and (28), which correspond very closely to the curves.

## The Limiting Cases of Very Thin and Very Thick Ceramics

For very thin ceramics, $\delta^2/(aT)$ or $(\delta^2/2a)\,(1/T + 1/T')$ is very nearly 0; then, according to Figure A-19, $\phi$ will be equal to one, and Equation (26) will be transformed into Equation (2). Thus, in terms of the zeroth eigenfunction solution, the thinner the ceramics, the more accurately applicable this simpler relationship becomes. Furthermore, Equation (28), as

well as an exactly determined limiting value (viz. appendix), shows that Equation (21) tends toward the expression,

$$\phi = \frac{2.142}{\delta}\sqrt{\frac{2a}{\frac{1}{T}+\frac{1}{T'}}} \quad \text{(for very thick ceramics)}, \tag{29}$$

as the thickness, $\delta$, of the ceramic increases. Correspondingly, Equation (26) assumes the following form,

$$\frac{1}{k_o} = (T+T')\left[\frac{1}{\alpha T}+\frac{1}{\alpha' T'}+\sqrt{\frac{1}{T}+\frac{1}{T'}}\,\frac{0.505}{\sqrt{\lambda c \gamma}}\right] \text{(for very thick ceramics)}. \tag{30}$$

The thickness of the ceramics no longer appears in this expression. Thus, the already mentioned requirement that, for very thick ceramics $k_o$ must be independent of ceramic thickness, is fulfilled.

The asymptotic representation [Equation (29)] is so good, that from $(\delta^2/2a)\,(1/T + 1/T') = 10$ on up, it is almost always possible to apply Equation (30) (with) satisfactory accuracy.

## Influence of the Dust Layer

The influence of the dust layer, which was first evaluated by Schack [14], can be calculated very simply through a slight extension of the theory that has been developed to this point.

A dust layer of thickness $\delta_o$ and thermal conductivity $\lambda_o$ is to be found on each of the two sides of the ceramic. If $\delta_o$ is so small that the thermal capacity of the dust layer can be neglected by comparison with the thermal capacity of the ceramic, then the entire heat given up by the gas must be transferred through the dust layer. Therefore, the heat arriving at the ceramic outer surface from the gas has not only overcome a thermal resistance proportional to $1/\alpha$ but also the resistance of the dust layer, which is proportional to $\delta_o/\lambda_o$. Thus, it is necessary to replace $1/\alpha$ by $1/\alpha + \delta_o/\lambda_o$ and $1/\alpha'$ by $1/\alpha' + \delta_o/\lambda_o$ in the earlier equations. In this way, Equation (26) for the heat transfer coefficient, $k_o$, is transformed into

$$\frac{1}{k_o} = (T+T')\left[\frac{1}{\alpha T}+\frac{1}{\alpha' T'}+\left(\frac{1}{T}+\frac{1}{T'}\right)\left(\frac{\delta}{6\lambda}\,\phi+\frac{\delta_o}{\lambda_o}\right)\right]. \tag{31}$$

By comparison with Equation (26), the essential factor expressing the influence of the dust layer in Equation (31) is, accordingly, the added term $\delta_o/\lambda_o$. In this respect it is to be borne in mind that the heat transfer coefficients, $\alpha$ and $\alpha'$ can have somewhat different values in the case of heat transfer to the dust layer than (exists) in the case of transfer to the dust-free outer surface of the ceramic.

## The Temperature Behavior at the Ends of the Regenerator and Its Influence on the Heat Exchange (Process)

As a rule, the zeroth eigenfunction very accurately represents the temperature changes within the inner regions of a regenerator. As already indicated, the processes (occurring) at the ends of the regenerator deviate from the trend of the zeroth eigenfunction. In accordance with the usual practical case, we assume that, as the case may be, the warmer as well as the cooler gas enters the regenerator at constant temperature. Then, for example, at the warm end of the regenerator, the temperature behaves basically as shown in Figure A-20. Again, the times are drawn in opposite directions in the warming and cooling periods. The uppermost curve, $\theta = \theta_1$, represents the temporally invariant entrance temperature of the warmer gas. The upper solid curves show the behavior of the outside surface and the mean temperature of the ceramic in the heating period. During the cooling period, the corresponding temperatures are $\theta'$, $\tau_o'$ and $\tau_m'$. The temperature of the cooler gas, $\theta'$, that exits here varies less with time than it does in the inner region of the regenerator. It is most noteworthy that the curves for $\tau_m$ and $\tau_m'$ are not coincident as in Figure 3, for example. The zeroth eigenfunction is unable to represent either the constant entrance temperature of the gas or the curved trend of $\tau_m$ and $\tau_m'$. To obtain an exact calculation, it is necessary to introduce the higher (order) eigenfunctions.

Certainly, it is possible to perform the calculation without the higher eigenfunctions if one ascertains the temperature behavior with respect to deviations from the zeroth eigenfunction by a temporal or other approximation process [15]. The effectiveness of the regenerator, which will be discussed later, can be calculated in this way. For practical numerical calculations, such methods may even be preferable. However, the physical relationship becomes clearest when one considers the higher eigenfunctions and investigates their influence on the heat exchange (process).

## On the Heat Transfer Coefficient Based on the Central Temperature of the Ceramic

Because the higher eigenfunctions behave in an essentially more complex way than the zeroth eigenfunction and because at most they play only the role of correction terms, it is possible to avoid them in a complete and exact determination of the local temperature variations in a ceramic cross section at each instant. Furthermore, it suffices to assume the difference between $\tau_o$ and $\tau_m$, and therefore between $\theta$ and $\tau_m$, at every instant to be equal to the time-averaged heat transferred per unit time calculated by means of the zeroth eigenfunction [16]. The temporal mean value of $\tau_o - \tau_m$ is

determined from Equation (20). If the quantity $\theta - \tau_o$, which is invariant in the case of the zeroth eigenfunction, is added to both sides of this equation, then

$$(\theta - \tau_m)_M = \left(\frac{1}{\alpha} + \frac{\delta}{6\lambda}\phi\right) \cdot \alpha \cdot (\theta - \tau_o)$$

is obtained as the temporal mean value of $\theta - \tau_m$. Furthermore, because $q = \alpha \cdot (\theta - \tau_o) \cdot T$ represents the quantity of heat transferred per unit area during one period, it is also possible to write, in place of the foregoing equation,

$$q = \bar{\alpha}\ (\theta - \tau_m)_M\ T, \tag{32}$$

if, for abbreviation, we set

$$\frac{1}{\bar{\alpha}} = \frac{1}{\alpha} + \frac{\delta}{6\lambda}\phi. \tag{33}$$

According to Equation (32), we can consider $\bar{\alpha}$ as a heat transfer coefficient based on the (temporal mean) temperature at the middle of the ceramic (cross section).

With this heat transfer coefficient, $\bar{\alpha}$, we will now calculate (dq) in the case of the higher eigenvalues at each point in time by writing

$$dq = \bar{\alpha}\ (\theta - \tau_m)\ dt, \tag{34}$$

for the quantity of heat transferred during the short time dt in place of Equation (32).

The error that is made by applying Equations (33) and (34) to the higher eigenfunctions plays only a very small role in the end results as the following consideration shows. It is unthinkable that, through the value of $\phi$ in Equation (33), the influence of the very rapid temperature changes immediately after the flow reversal will be, to some degree, uniformly distributed through the total duration of the period, particularly for the calculation of the heat transfer coefficient (which is our ultimate goal). From this point of view, it appears at first that very noticeable errors (will) occur in the case of the higher eigenfunctions because the gas and ceramic temperatures as determined by these functions behave essentially

differently than the zeroth eigenfunction. Therefore, it cannot be expected that the higher eigenfunctions will be well approximated by Equation (34). However, for the accuracy of the final result, only the magnitude of the error in suitably formed sums, yet to be more precisely discussed, of the higher eigenfunctions is significant. It was shown in an earlier publication [17] for the case $\phi = 1$ that this error is small and, even in unfavorable cases, affects the total quantity of heat transferred in the regenerator by less than 1%. In the case $\phi < 1$, even smaller errors are to be expected because then, according to Equation (20), even the temperature difference $\tau_o - \tau_m$ is smaller, and an inaccuracy in calculating it is correspondingly less important.

The introduction of $\bar{\alpha}$ in the case of the higher eigenfunctions makes it possible to calculate (the heat transfer) as if the temperature of the regenerator core at a given cross section and given instant had the uniform temperature, $\tau_m$, and as if the temperature difference, $\theta - \tau_m$, corresponding to the heat transfer to the outer surface, were at one's disposal. This limiting case of uniform temperature over the entire cross section is applied with very good accuracy to the regenerators of low-temperature technology because these regenerator cores are fabricated from thin plates of high thermal conductivity instead of ceramic. In his first report on regenerators [18] the author derived the equations for all the eigenfunctions corresponding to this case. The calculation with $\bar{\alpha}$ and $\tau_m$, therefore, allows these equations also to be used without change in current considerations. Even if the already mentioned approximate methods are used instead of the higher eigenfunctions, the introduction of $\bar{\alpha}$ is necessary because even these processes have been developed for uniform temperatures in the ceramic cross section.

It should also be mentioned that, in the case of the dust-covered ceramic outer surface, Equation (33), corresponding to the foregoing considerations, is to be replaced by

$$\frac{1}{\bar{\alpha}} = \frac{1}{\alpha} + \frac{\delta}{6\lambda}\,\phi + \frac{\delta_o}{\lambda_o}\,. \qquad (33a)$$

## The Higher Eigenfunctions

.
.
.

The paper continues, but translation is terminated at this point.

NOTES

0. Extended edition of a contribution of the author to the Convention of the VDI - Committee for Thermal Research on 13 October 1941 in Dresden. See also the contribution to the convention by E. Schmidt in Z. VDI, 86, 9/10 (1942) pp. 135-138.

1. W. Heiligenstaedt, "Die Berechnung von Wärmespeichern," Arch. Eisenhüttenw., 2 (1928/29) pp. 217-222; also W. Heiligenstaedt "Regenoratoren, Rekuperatoren, Winderhitzer," Leipzig (1931).

2. K. Rummel, "Die Berechnung der Wärmespeicher auf Grund der Wärmedurchgangzahl," Stahl und Eisen, 48 (1928) pp. 1712-1715.

3. In an earlier work, Heiligenstaedt has also discussed the case of the temporal variation of the gas temperatures, cf. W. Heiligenstaedt, "Beitrag zur Berechnung von Winderhitzern und Regeneratoren," Diss. Aachen (1924) or p. 169 of the book mentioned in Note 1, above: "Regeneratoren, Rekuperatoren, Winderhitzer."

4. H. Hausen, "Berechnung der Steintemperatur in Winderhitzern," Arch. Eisenhüttenw., 12 (1938/39) pp. 473-480.

5. H. Hausen, op. cit. p. 479 (Abschnitt: Erweiterung des Berechnungsverfahren).

6. I thank Dr. A. Schack in Düsseldorf for the encouragement to develop the extended theory presented here. Dr. Schack mentioned Equation (18) (corresponding to Equation (2) of this discussion) derived in my publication noted in footnote 4, in his book Der industrielle Wärmeaustausch 2nd ed. Düsseldorf (1940) pp. 224 and 245. This has led to a long correspondence with me concerning questions raised there. As it has turned out, his objection to my equation is only that it does not apply even to thin ceramics in those cases where the deviating temperature behavior at the ends of the regenerator exerts a strong influence but is not considered in the calculation.

7. See for example the publication of E. Schmidt in "Beiträge zur technischen Mechanik und technischen Physik," Festschrift August Föppl zum 70 Geburtstag Berlin (1924) or H. Gröber and S. Erk, Die Grundgesetze der Wärmeübertragung, 2nd ed., Berlin (1933) p. 92.

8. K. Rummel, op. cit.; K. Rummel and A. Schack, Stahl und Eisen, 49 (1929) pp. 1300-1311; Arch. Eisenhüttenw., 2 (1928/29) pp. 473-479; see also A. Schack, Arch. Eisenhüttenw., 2 (1928/29) pp. 481-486 and K. Rummel, Arch. Eisenhüttenw., 4 (1930/31) pp. 367-374.

9. If desired, this influence can be subsequently and separately considered. The author has presented a simple method suited to these conditions at the Convention of the Study Group "Kältentechnik" of the VDI in Prague on 23 May 1941. See also K. Nesselmann, "Der Einfluss der Wärmeverluste auf Doppelrohrwärmeaustauscher," Z. ges, Kälte-Ind., 35 (1928) p. 62.

10. For the simplest case, W = W' and T = T'; this follows from Equations (46) and (47) of the following publication: H. Hausen, Über die Theorie des Wärmeaustausches in Regeneratoren," Z.a.M.M., 9 (1929) pp. 173-200. Compare Equations (35) and (40) of the above article.

11. Mathematically, it is worth mentioning that the two members of Equation (9) that include $(\partial\tau_m/\partial t)_f$ can also be considered to be the zeroth member of the cosine series, as can be shown easily through a limiting process by allowing $\beta_n \longrightarrow 0$ as $B_n \longrightarrow \infty$.

12. viz., e.g., B. W. Hort and A. Thoma, Die Differentialgleichungen der Technik u. Physik, A. Barth, Leipzig (1939) p. 342.

13. K. Schumacher, "Grossversuche an einer zu Studienzwecken gebauten Regenerativekammer," Arch. Eisenhüttenw., 4 (1930/31) pp. 63-74.

14. A. Schack, "Über den Einfluss des Stabbelages auf den Wirkungsgrad von Regeneratoren," Z. Techn. Phys., 9 (1928) pp. 390-398; Arch. Eisenhüttenw., 2 (1928/29) pp. 287-292.

15. H. Hausen "Näherungsverfahren zur Berechnung des Wärmeaustauches in Regeneratoren," Z.a.M.M., 11 (1931) pp. 105-114; see also H. Hausen, "Wärmeaustauch in Regeneratoren," Z. VDI, 73 (1929) p. 431.

16. The following consideration was already (though) less precisely and less generally presented in the earlier publication (cf. Notes 4 and 5).

17 H. Hausen, op. cit. (cf. Notes 4 and 5) Figure 16.

18. H. Hausen, "Über die Theorie des Wärmeaustauches in Regeneratoren," Z.a.M.M., 9 (1929) pp. 173-200.

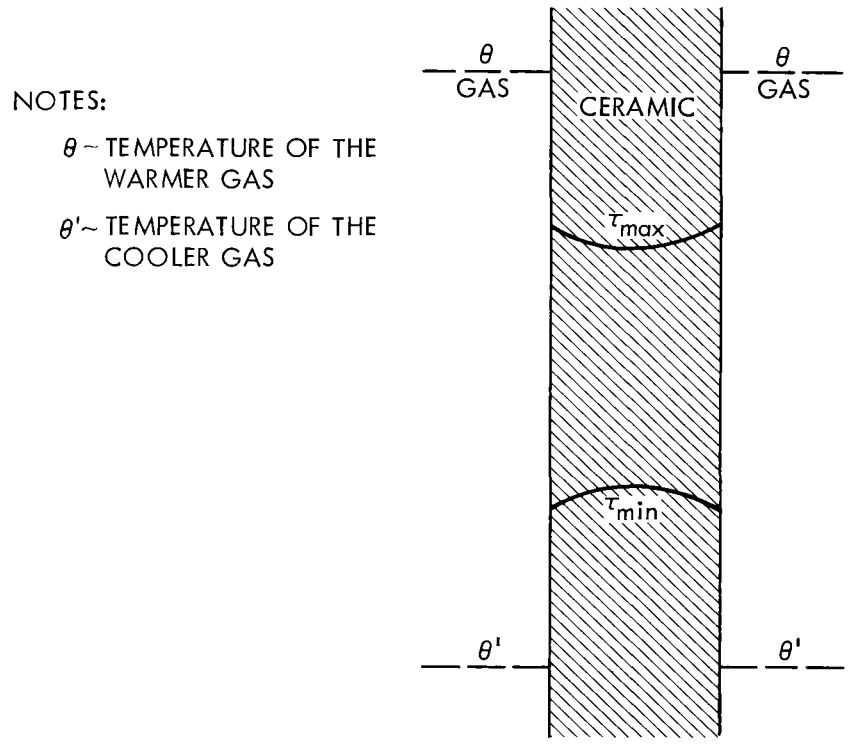


Figure A-1. Oscillation of the Ceramic Temperature of a Regenerator Between $\tau_{max}$ and $\tau_{min}$

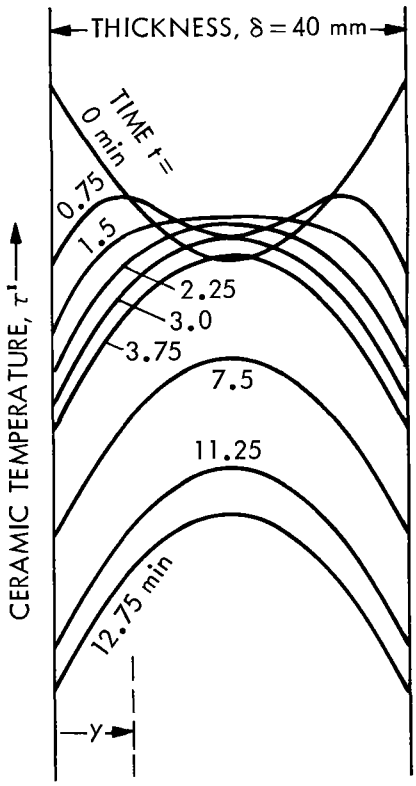


Figure A-2. Temperature Behavior in a Ceramic of Thickness δ During the Cooling Period

LEGEND:

HEATING PERIOD:

$\tau_o$ ~ OUTER SURFACE TEMPERATURE OF THE CERAMIC

$\tau_m$ ~ LOCAL MEAN OF THE CERAMIC TEMPERATURE

$t$ ~ TIME

COOLING PERIOD:

$\tau'_o$ ~ OUTER SURFACE TEMPERATURE OF THE CERAMIC

$\tau'_m$ ~ LOCAL MEAN OF THE CERAMIC TEMPERATURE

$t'$ ~ TIME

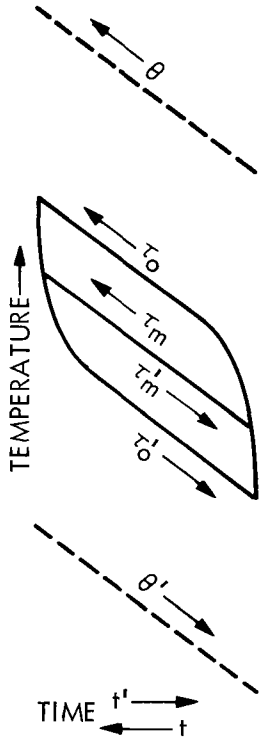


Figure A-3. Actual Temperature Behavior in the Ceramic

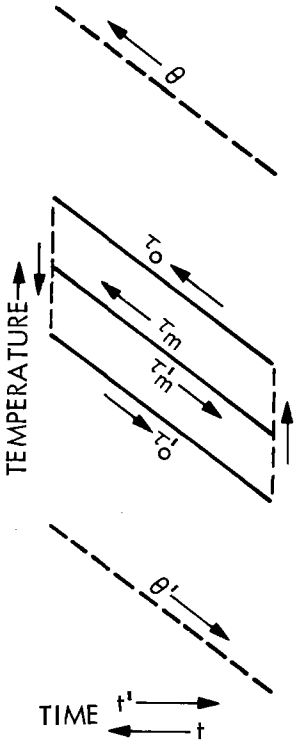


LEGEND:

HEATING PERIOD:

$\tau_o$ ~ OUTER SURFACE TEMPERATURE OF THE CERAMIC

$\tau_m$ ~ LOCAL MEAN OF THE CERAMIC TEMPERATURE

$t$ ~ TIME

COOLING PERIOD:

$\tau'_o$ ~ OUTER SURFACE TEMPERATURE OF THE CERAMIC

$\tau'_m$ ~ LOCAL MEAN OF THE CERAMIC TEMPERATURE

$t'$ ~ TIME

Figure A-4. Previously Assumed Temporal Temperature Behavior in the Ceramic

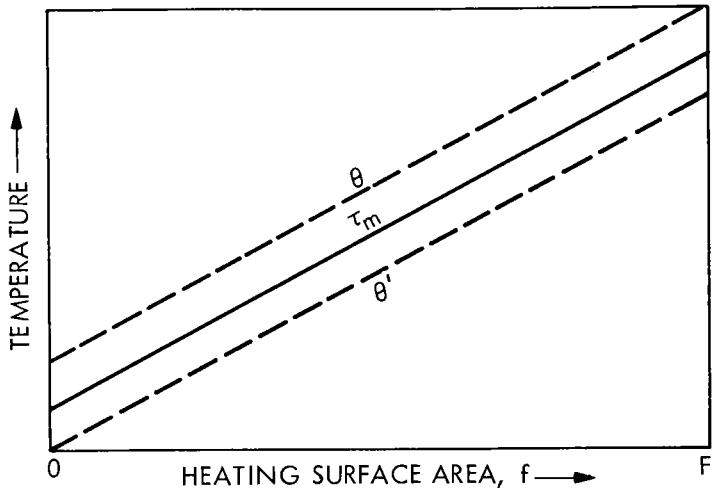


Figure A-5. Temperature Behavior in a Recuperator for Equal Thermal Capacity of the Two Gases (W = W')

NOTES:

DURATION OF HEATING AND COOLING PERIODS: 1 h EACH

y ~ DISTANCE FROM THE CERAMIC OUTER SURFACE

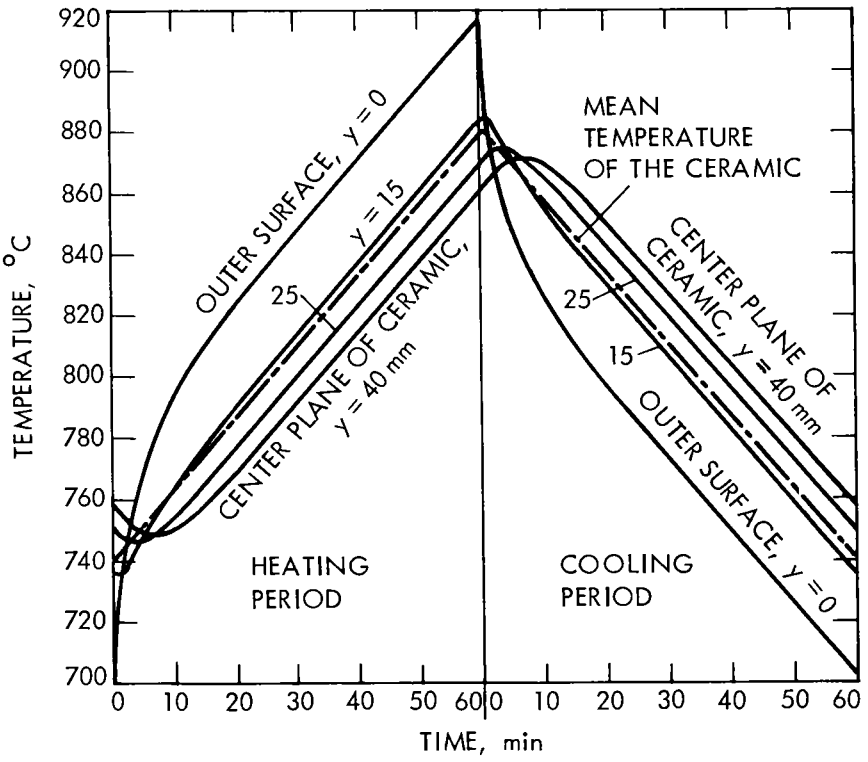


Figure A-6. Calculated Temperature Behavior in an 80-mm-Thick Regenerator Ceramic (Cross Section) (See also Figure A-7)

NOTES:

DURATION OF COOLING PERIOD: 1 h

y ~ DISTANCE FROM ONE OF THE TWO CERAMIC OUTER SURFACES

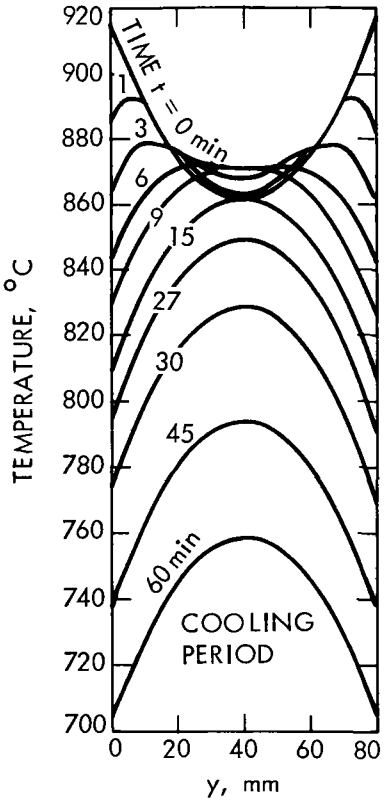


Figure A-7. Calculated Temperature Behavior of an 80-mm-Thick Regenerator Ceramic (Cross Section) (See also Figure A-6)

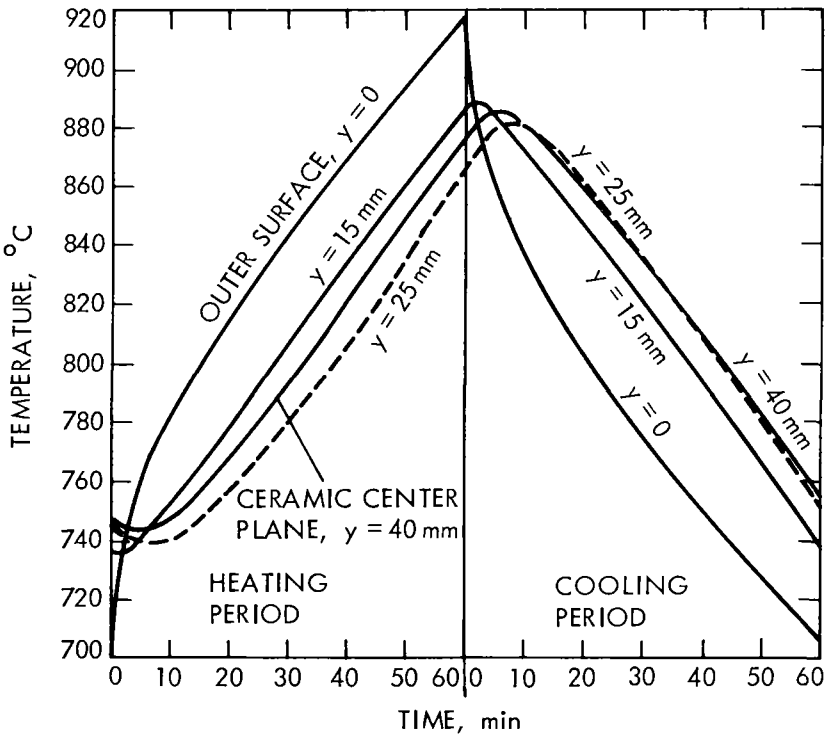


Figure A-8. Measured Temperature Behavior in an 80-mm-Thick Regenerator Ceramic (According to K. Schumacher)

LEGEND:

$\delta$ ~ CERAMIC THICKNESS

$\tau$ ~ DURATION OF THE HEATING PERIOD

$\tau'$ ~ DURATION OF THE COOLING PERIOD

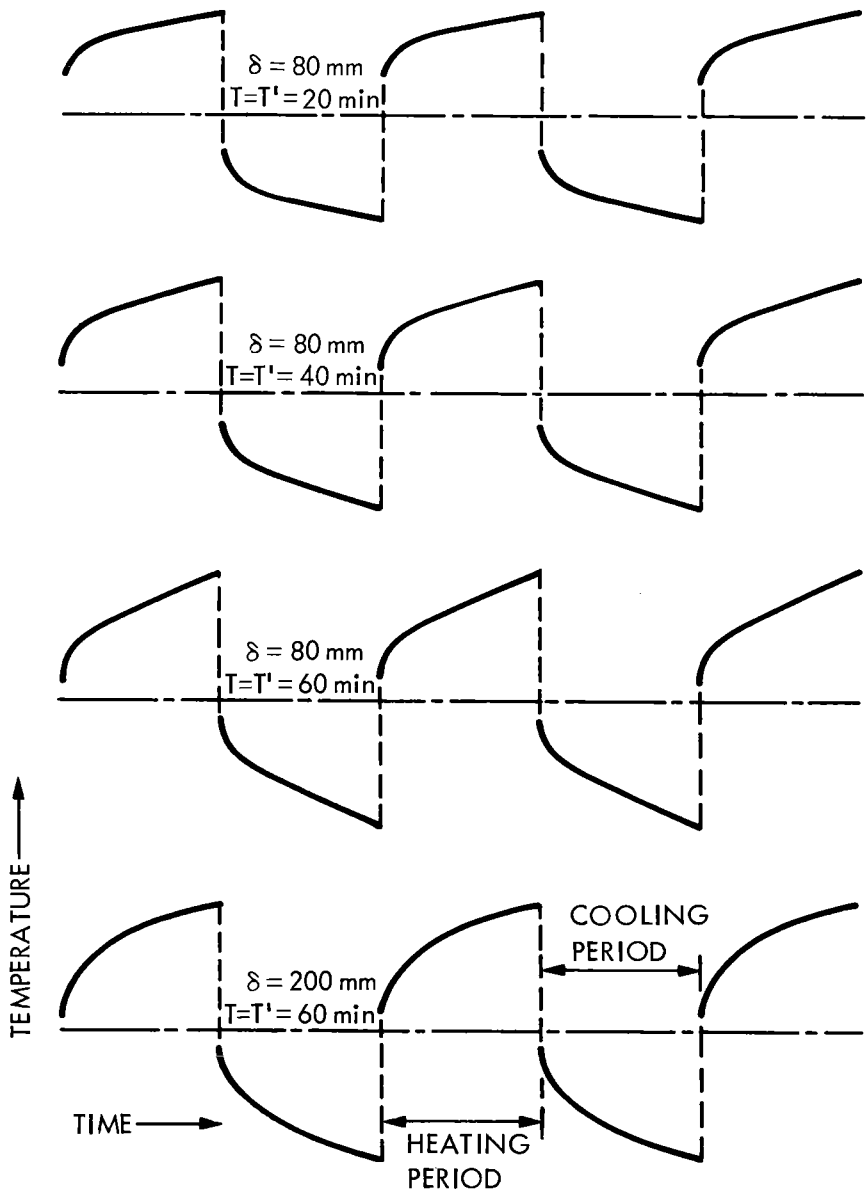


Figures A-9 through A-12. Calculated Temporal Behavior of the Gas Temperatures in a Regenerator. Heat transfer coefficients in the heating and cooling periods are $\alpha = \alpha' = 20$ kcal/($m^2 h\,^oC$).

LEGEND:

$\delta$ ~ CERAMIC THICKNESS

$\tau$ ~ DURATION OF THE HEATING PERIOD

$\tau'$ ~ DURATION OF THE COOLING PERIOD

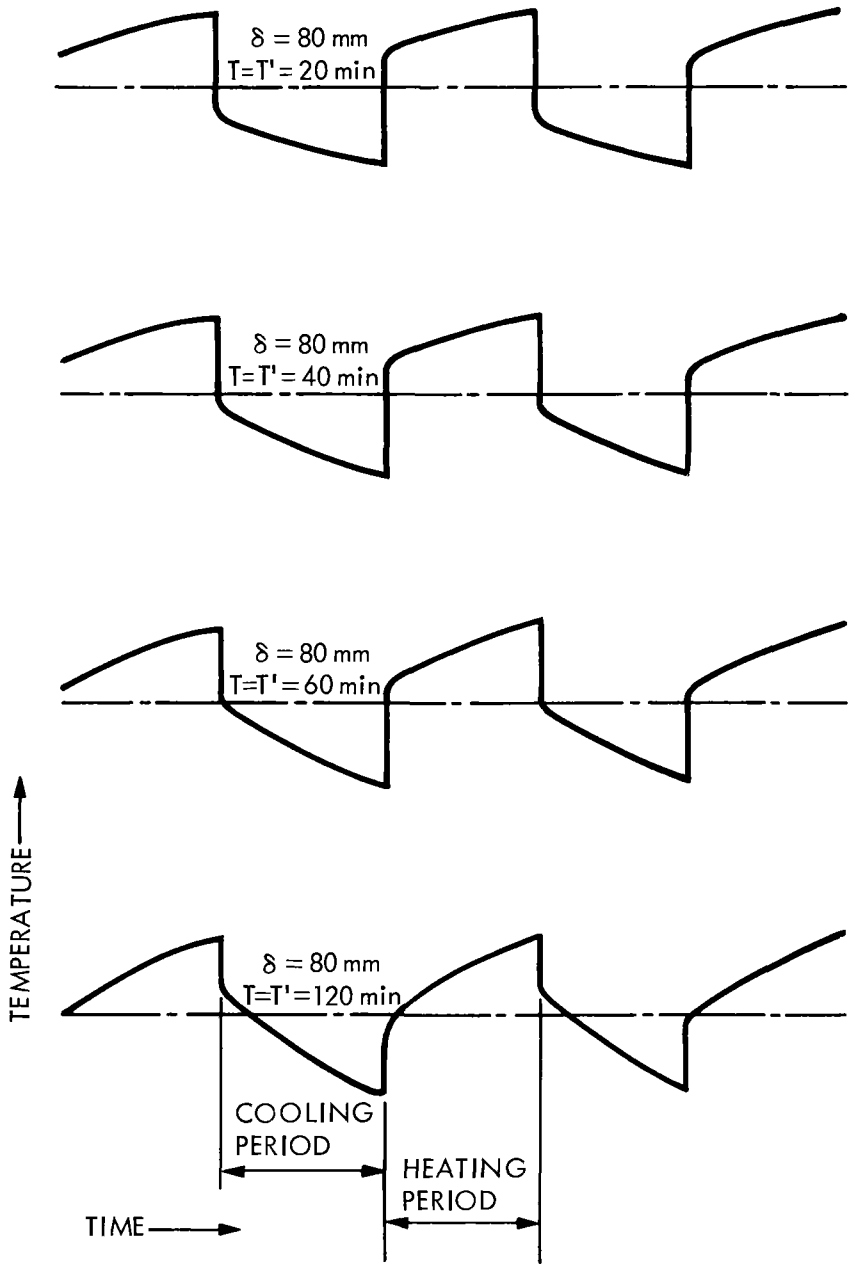


Figures A-13 through A-16. Measured Temporal Behavior of the Gas Temperatures in a Regenerator

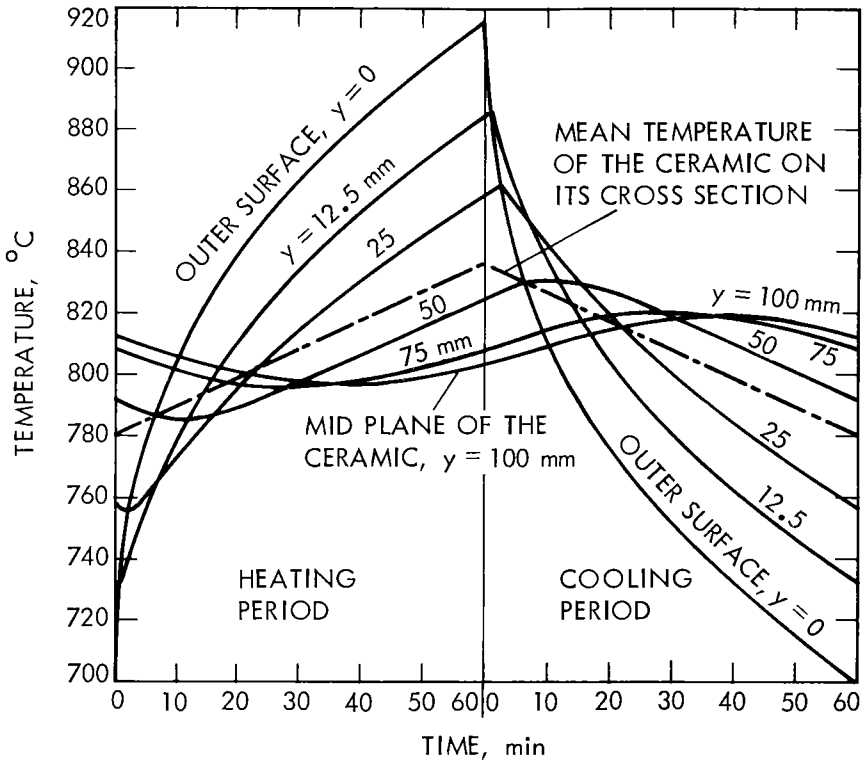


NOTES:

DURATION OF HEATING AND COOLING PERIODS: 1 h EACH

y ~ DISTANCE FROM THE CERAMIC OUTER SURFACE

Figure A-17. Temperature Behavior in a 200-mm-Thick Regenerator Ceramic (See also Figure A-18)

NOTES:

DURATION OF COOLING PERIOD: 1 h

y ~ DISTANCE FROM ONE OF THE TWO CERAMIC OUTER SURFACES

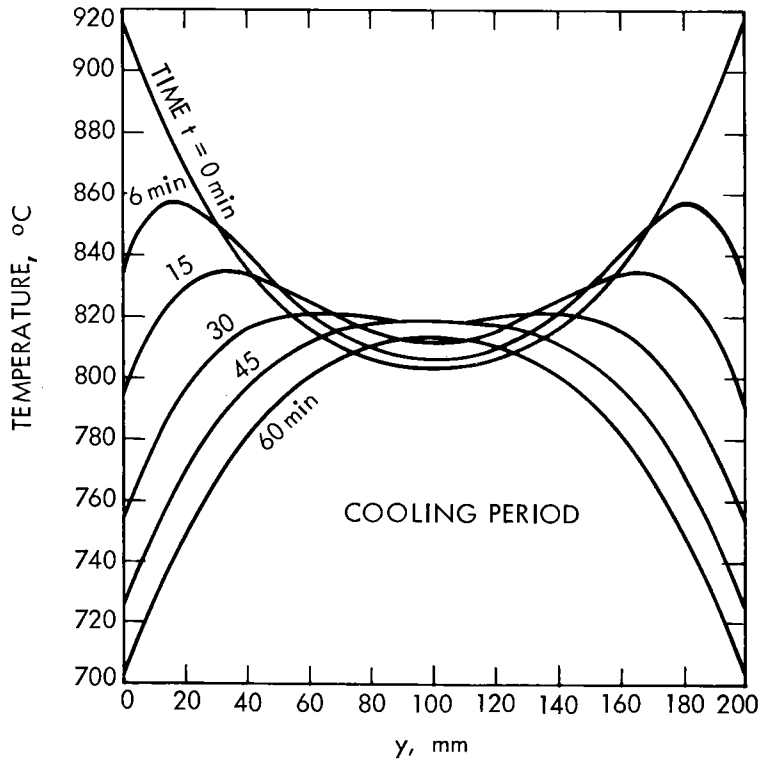


Figure A-18. Temperature Behavior in a 200-mm-Thick Regenerator Ceramic (See also Figure A-19)

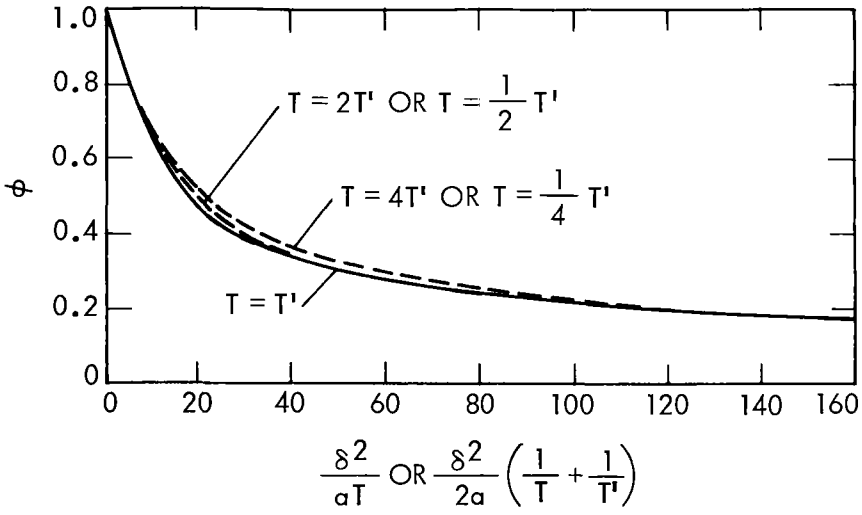


Figure A-19. $\phi$ as a Function of $\delta^2/aT$ or $(\delta^2/2a)(1/T + 1/T')$ as the Case May Be. (Required for the calculation of the heat transfer coefficient, $k_o$, for regenerators using Equation (26).) The value of Equation (21) can be obtained from the figure.

LEGEND:

$\theta$ ~ TEMPERATURE OF THE GAS IN THE WARMING PERIOD

$\theta'$ ~ TEMPERATURE OF THE GAS IN THE COOLING PERIOD

$\tau_o$ ~ OUTER SURFACE TEMPERATURE OF THE CERAMIC IN THE HEATING PERIOD

$\tau_o'$ ~ OUTER SURFACE TEMPERATURE OF THE CERAMIC IN THE COOLING PERIOD

$\tau_m$ ~ MEAN TEMPERATURE OF THE CERAMIC (OVER A CROSS SECTION) IN THE HEATING PERIOD

$\tau_m'$ ~ MEAN TEMPERATURE OF THE CERAMIC (OVER A CROSS SECTION) IN THE COOLING PERIOD

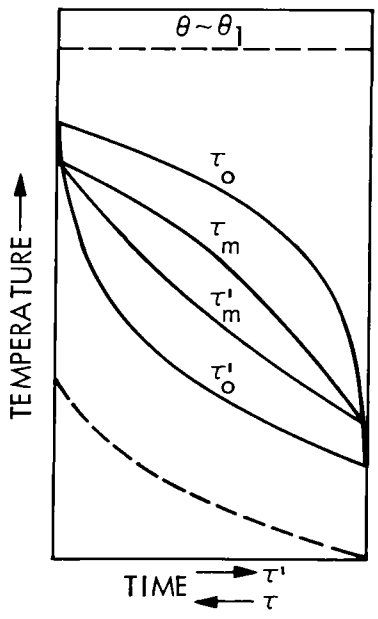


Figure A-20. Temporal Temperature Behavior at the Warm End of the Regenerator